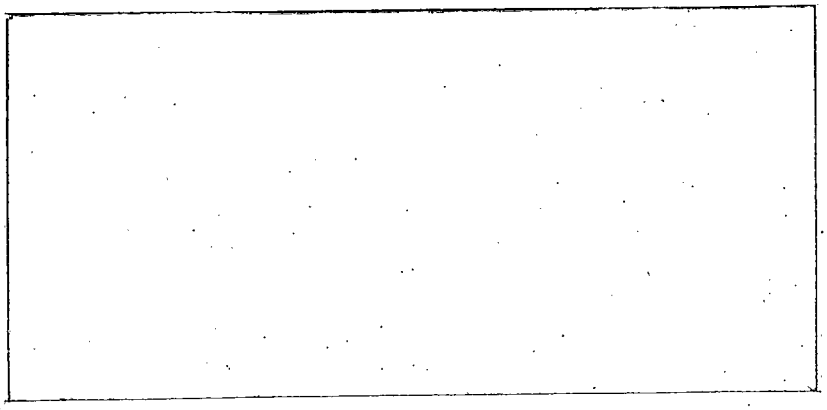

Materials Science Center

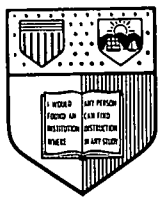

Cornell University
ITHACA, NEW YORK
14850

DISCLAIMER

Report #2072

#C00-3151-30

ABSORPTION SPECTRA OF GLASSES IN THE FAR INFRARED

by

Charles L. Cabrera

MS Thesis
January, 1974

Research Group:
Prof. A. L. Sievers
LASSP

ACKNOWLEDGMENTS

The author wishes to sincerely thank Professor A. J. Sievers for his guidance during this work. Without his constant interest, enthusiasm, and valuable help this work would never have been possible. Thanks is given to G. Schmidt who grew some of the glass samples and to D. Tanner for his initial help in working with the experimental equipment. Special thanks is given to T. Maloney for proofreading several parts of this thesis and to D. Elsley for his many helpful discussions. The author is grateful to Professor R. Pohl and Professor N. Mermin for serving on his special committee, and to the staff of Cornell's Materials Science Center and Laboratory of Atomic and Solid State Physics.

The author considers himself very fortunate to have been able to work with Professor Sievers and the far infrared group. This was a group more of friends than of co-researchers. This is exemplified by the group ski trips, group lunches, group pingpong matches, and the group discussions over beer. It was always fascinating to hear Professor Sievers' stories and his discussions on "beer" lines. Even D. Elsley's science fiction stories were sometimes interesting. The author will never forget the great guys who made up the far infrared group.

This work has been supported by the U.S. Atomic Energy Commission through contract no. AT(11-1) 3151, Technical Report no. COO-3151-30.

TABLE OF CONTENTS

LIST OF FIGURES

ABSTRACT

Precise measurements have been made of the far infrared absorption coefficient of several glasses, vitreous silica, GeO_2, and $CaK(NO_3)_3$. Measurements were made by Fourier transform spectroscopic techniques which employed a Michelson or a lamellar-grating interferometer. Except for temperature dependence runs, the samples were all at 4.2°K and a helium-3 cooled (0.3°K) germanium bolometer was used as a detector. In arriving at the absorptivity, multiple reflections within the sample were considered.

The three glasses have absorption coefficient vs. frequency curves which are qualitative similar, although they differ in absolute magnitude. When graphed as the absorptivity divided by the frequency squared the various spectra had several anomalies. For vitreous silica peaks in $\alpha(\omega)/\omega^2$ at 40 cm^{-1} and 3 cm^{-1} were measured. The peak at 40 cm^{-1} is similar to that obtained by other investigators. The peak at 3 cm^{-1} was measured for the first time. For GeO_2 the peak occurred at 34 cm^{-1} and is similar in shape to that obtained by other researchers. For $CaK(NO_3)_3$ the low peak was around 4 cm^{-1}.

Several theoretical models have been proposed to explain the far infrared absorption of glasses. One predicts that, as a function of the frequency, the absorptivity

divided by the frequency squared should closely resemble the density of states. A comparison of a density of states derived from far infrared data to one derived from heat capacity measurements for vitreous silica indicates that both have peaks around 40 cm^{-1}, but only the absorptivity measurements show another peak at 3 cm^{-1}. Another model which describes the absorption in terms of defects in the glass does not fit the experimental results. Finally the predictions of a tunneling model were tested by studying the temperature dependence of the absorption coefficient.

CHAPTER I

HISTORY OF DISORDERED SYSTEMS

A. Introduction

Specific heat measurements[1,2] at low temperatures have demonstrated that an anomalously large number of low lying states occur in glasses below a frequency of 10 cm^{-1}. Thermal conductivity measurements which probe the same frequency interval have shown that all glasses scatter thermal phonons in a charactersitic manner.[1,2] The electromagnetic absorption spectrum of disordered insulating glasses has not yet been measured in this extreme far infrared region below 10 cm^{-1}. The purpose of this thesis is to close the gap between the infrared and the microwave measurements on glasses to see if a characteristic absorption spectrum is associated with disordered materials.

B. Specific Heat and Heat Conduction

Measurements on the thermal conductivity and the specific heat of glasses have shown that for these properties a characteristic feature can be associated with disordered systems. Specifically the same conductivity has been observed in all silica based glasses![1] These samples vary in composition from pure SiO_2 (vitreous

silica) to borosilicate glass (pyrex), to soda-lime glass (soft glass). Even in vastly different materials like polymers, elemental amorphous solids, and partially crystallized glass ceramics (pyroceran) the thermal conductivity does not differ by more than one order of magnitude from that of silica glass.

Stephens[2] has also found that a formula for the specific heat given by $C_v = c_1T + c_3T^3$ can be applied to samples as diverse as: As_2S_3, B_2O_3, $3SiO_2 \cdot Na_2O$, GeO_2, Ge No. 7031 Varnish, SiO_2, Pyrex, Se, Polymethyl Methacrylate (PMMA), PS, Lexan, and Glycerol (Figure 1.1). This uniformity of thermal properties among the diverse group of glasses leads to the conclusion that the mechanism determining the heat conduction and specific heat in these solids must depend on properties shared by all non-crystalline solids and not on any particular materials.

C. Previous Work on Electromagnetic Absorption of Glasses

1. Infrared

In 1920 Grantham[3] at Cornell measured the infrared transmission from 0.6 μ to 4.0 μ of four glasses at three different temperatures (80°C, 307°C, 440°C). Grantham states that "These glasses have transmission curves which are very similar...." even though they are of different chemical composition. Recent measurements on the infrared transmission of glasses[4] have shown that for a wide variety of glasses the transmission spectra are somewhat

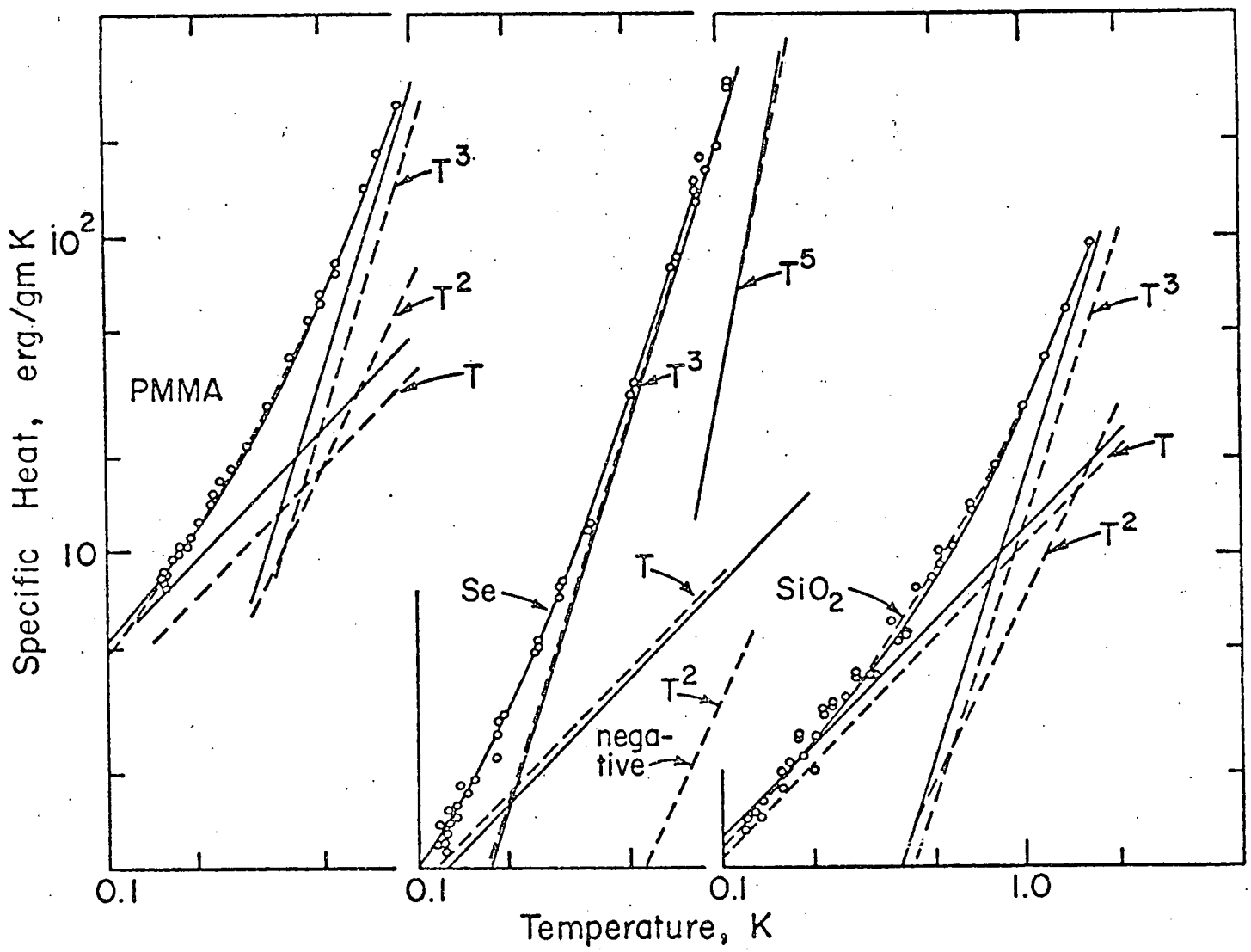

Figure 1.1 Polynomial fits to specific heat data for SiO_2, Se, and PMMA, after R. B. Stephens.[2] The solid lines are the components and sum of the fit $e_v = c_1T + c_3T^3$. The dotted lines are the components and sum of the fit $c_v = c_1T + c_2T^2 + c_3T^3$.

similar as shown in Figure 1.2. We see that the transmission increases steadily in the range from 0.2 μm to 0.34 μm (the absorption decreases), is fairly constant from 0.34 μm to 2.2 μm, and then decreases (absorption increases) to at least 5.0 μm. The absorption remains very large until we reach the far infrared region.

2. Far Infrared

In the far infrared region one of the first measurements of the absorption of glasses was made by Stolen[5] in 1968. His measurements of the room temperature far-infrared absorption of vitreous silica (fused Quartz) show an absorption proportional to the square of the frequency above 30 cm^{-1} and a sharp decrease below 30 cm^{-1}. Stolen explains the square dependence has been due to defects in the continuous, no defects, glass. To explain the sharp decrease below 30 cm^{-1} he had to assume some correlation among the defects.

In a later more sensitive measurement on vitreous silica Stolen[6] shows that the absorption does not vary as the frequency squared even above 30 cm^{-1}. His data when plotted as $\alpha(\omega)/\omega^2$ vs. ω, is shown in Figure 1.3. A maxima occurs at 42 cm^{-1} and a minima at 10 cm^{-1}. These measurements are more precise because in arriving at the absorptivity Stolen takes into account the effect of multiple reflections within the sample. From his data one notes that below 15 cm^{-1} there is a difference between his measurements at room temperature (300°K) and those at

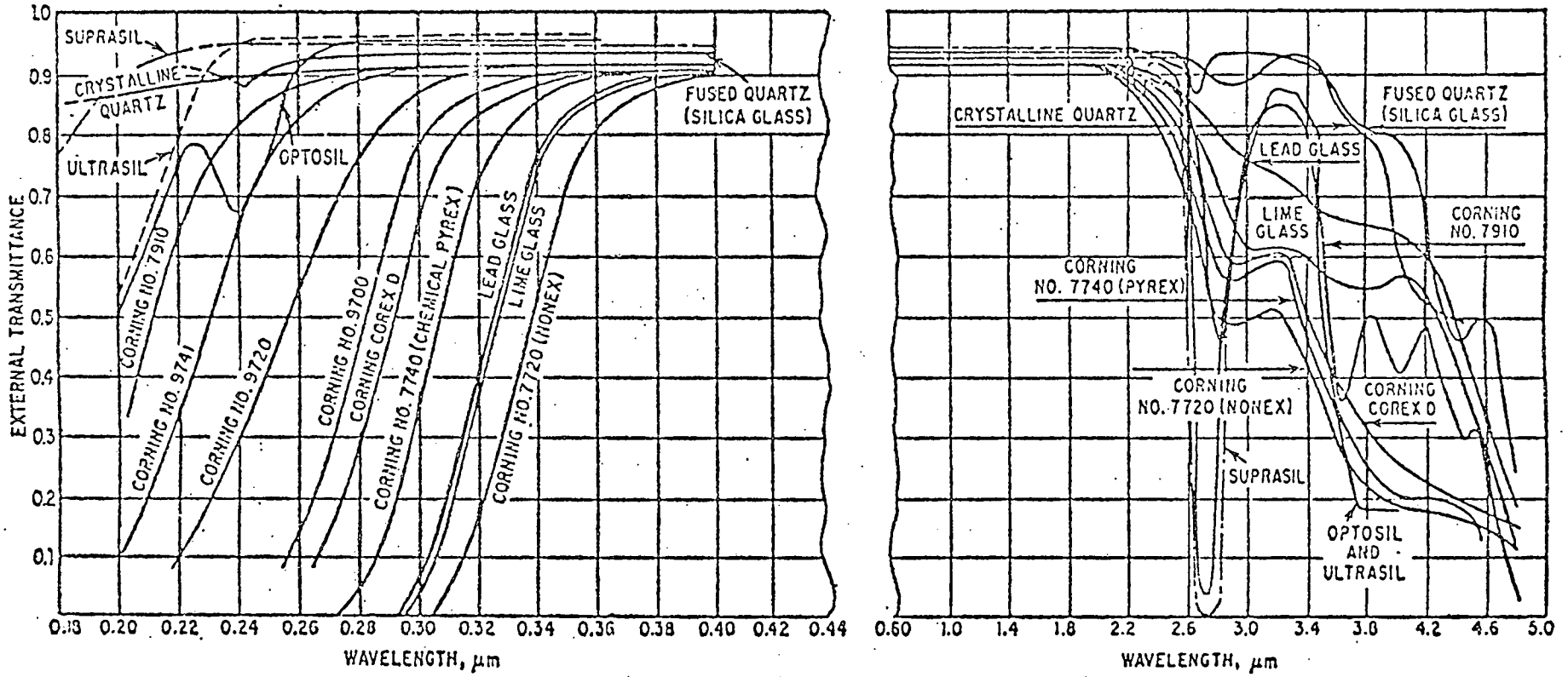

Figure 1.2 The external transmittance vs. wavelength of several samples of Corning and Amersil glasses in the infrared.

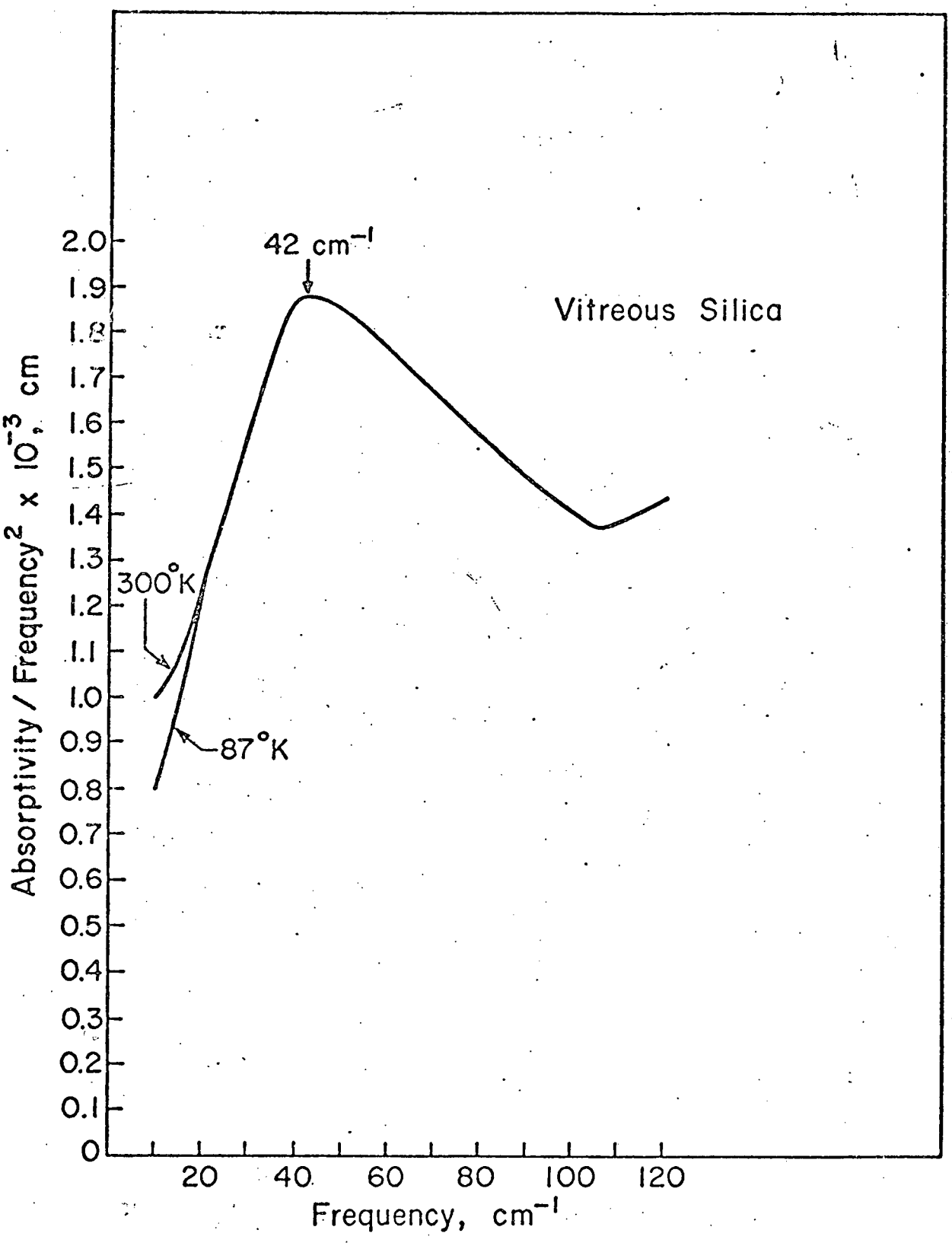

Figure 1.3 The absorption coefficient of vitreous silica at 87°K and 300°K plotted as $\alpha(\omega)/\omega^2$ vs. ω, after R. Stolen.[6]

87°K thereby implying a decrease in absorption with a decrease in temperature. Above 15 cm^{-1} there is no difference in the absorption between the two temperatures. Stolen also measured the absorption coefficient of GeO_2 and B_2O_3 and found corresponding maximas in $\alpha(\omega)/\omega^2$ at 38 cm^{-1} and 26 cm^{-1} respectively (see Figure 1.4). Note that the spectrums are very similar for the three different glasses.

Wong and Whalley[7] have also measured the far infrared absorptivity of vitreous silica in the region from 100 cm^{-1} to 15 cm^{-1} at 300°K and 100°K. Their data in Figure 1.5 shows that above 18 cm^{-1} the absorptivity is independent of temperature and is "...undoubtably caused by fundamental vibrations". A theory they propose suggests that the absorption coefficient divided by the frequency squared should be closely related to the density of vibrational states. Their data is very similar to that of Stolen,[6] where their maxima in $\alpha(\omega)/\omega^2$ occurs at 38 cm^{-1}. The magnitudes of $\alpha(\omega)/\omega^2$ at the maxima are 1.87 cm for Stolen and 2.13 cm for Whalley. Like Stolen they also measured a decrease in absorption with a decrease in temperature for frequencies below 18 cm^{-1}.

3. Microwave

There have been some meausrements of the microwave dielectric loss in glass which is directly proportional to the absorption coefficient. The coefficient is given by the following relation: $\alpha(\omega) = 2\pi n\omega \tan \delta$ where n is

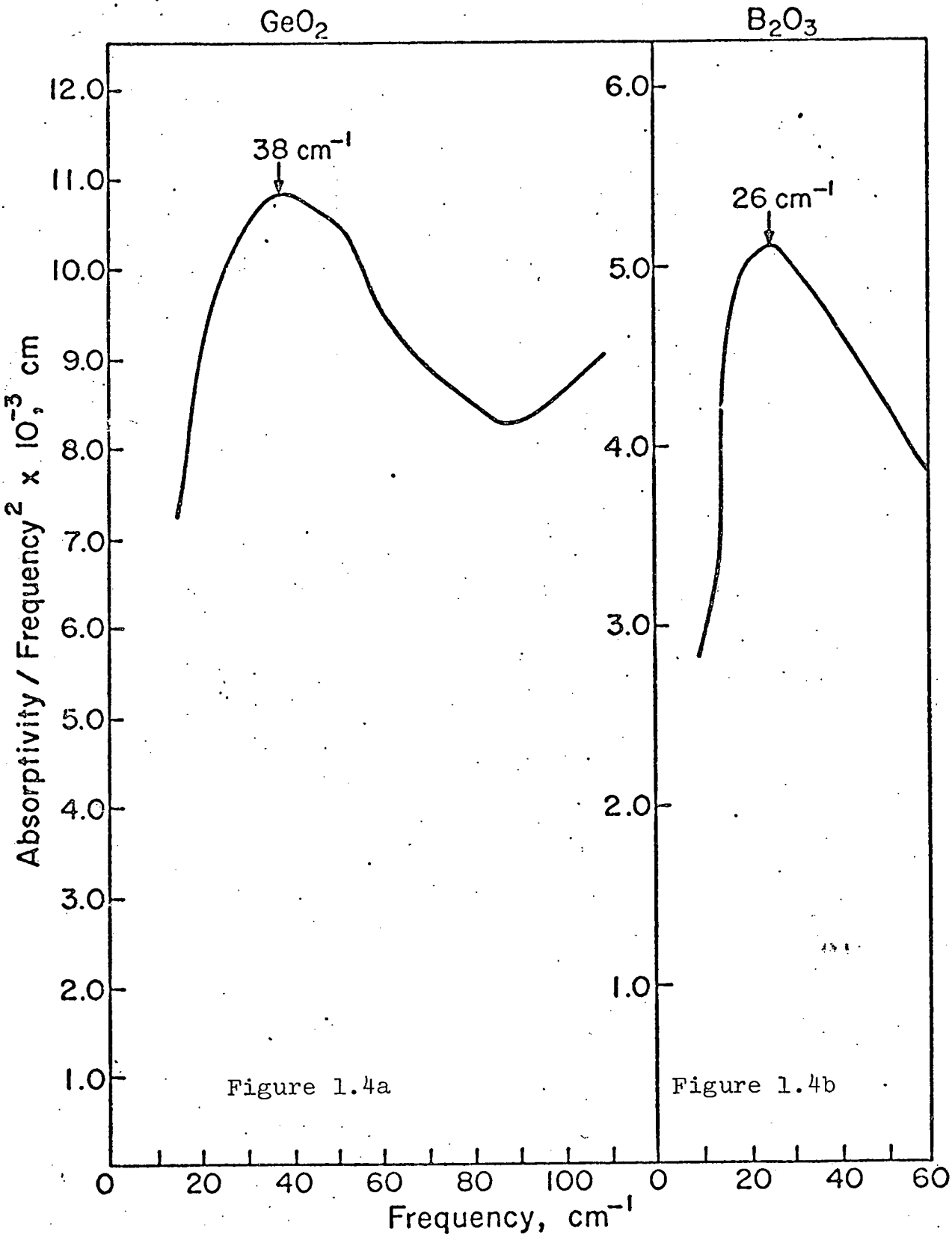

Figure 1.4a

Figure 1.4b

Figure 1.4 The absorption coefficient of GeO_2 and B_2O_3 at room temperature plotted as $\alpha(\omega)/\omega^2$ vs. ω, after R. Stolen.[6]

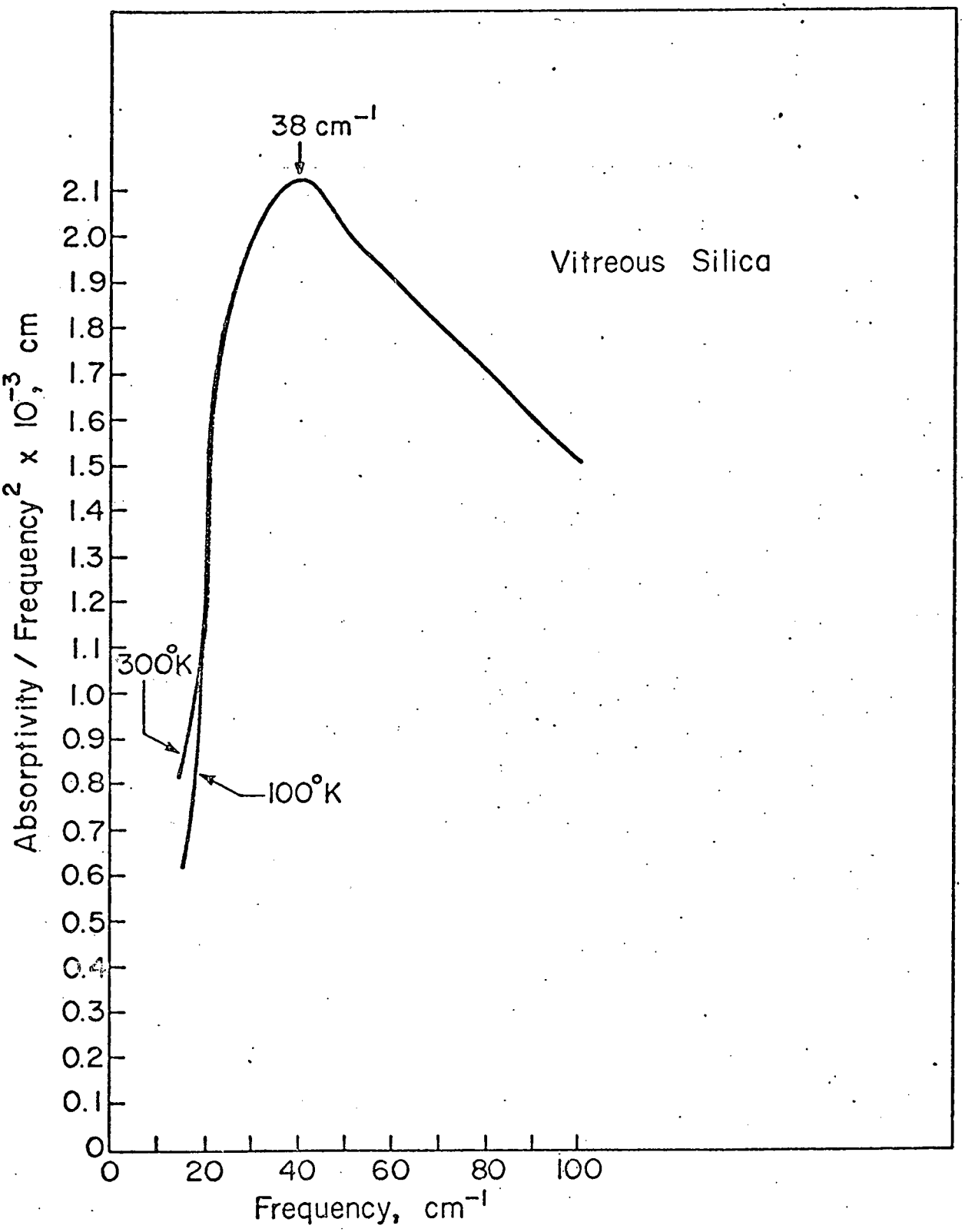

Figure 1.5 The absorption coefficient of vitreous silica at 100°K and 300°K plotted as $\alpha(\omega)/\omega^2$ vs. ω, after P.T.T. Wong and E. Whalley.[7]

the refractive index and ω is given in wave numbers. One such measurement was done by Amrhein and Muller.[8] Their measurements of the dielectric loss of vitreous silica at 32 GHz (1.06 cm^{-1}) between 4.2 and 300°K are shown in Figure 1.6a. Their measurements show an increase in the dielectric loss (or the absorption) with an increase in temperature from 1°K to 100°K.

Other measurements of the dielectric loss were performed by Volger and Stevels.[9] They measured the temperature dependence of the dielectric loss for different samples (made by different companies) of fused quartz at 32 KHz from 14°K to 300°K. We can see (Figure 1.6b) that the tan δ vs. T curves of nearly all the samples have the same qualitative appearance. For measurements of the dielectric loss over a wide range of frequencies, from 10^2 to 10^{10} Hz, one is referred to Table 5d-8 in the American Institute of Physics Handbook.[10]

D. Remarks on Theory

The far infrared absorption spectrum associated with the lattice vibrational modes of an ordered crystal is now fairly well understood.[11] For a pure ordered crystal a few well defined optically active modes are observed in the infrared.[12,13] To first order these modes correspond to what is usually referred to as the reststrahlen region. This is the region between the transverse optic branch (TO) and the longitudinal optic branch (LO) and the crystal is opaque in this region. At frequencies outside the

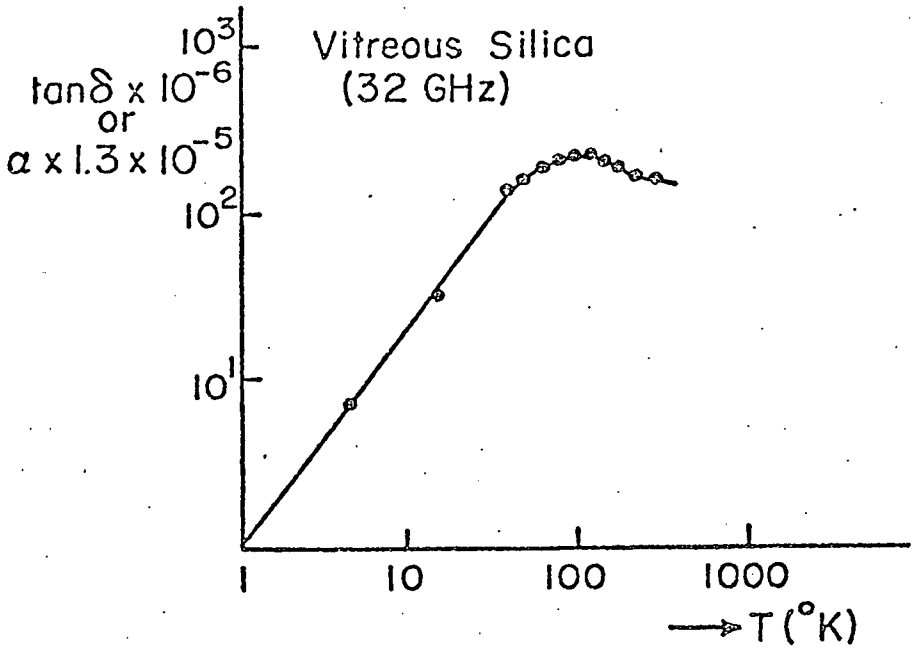

Figure 1.6a The absorption coefficient vs. temperature for vitreous silica at 32 GHz (1.06 cm^{-1}), after E.M. Amrhein and F. H. Muller.[8]

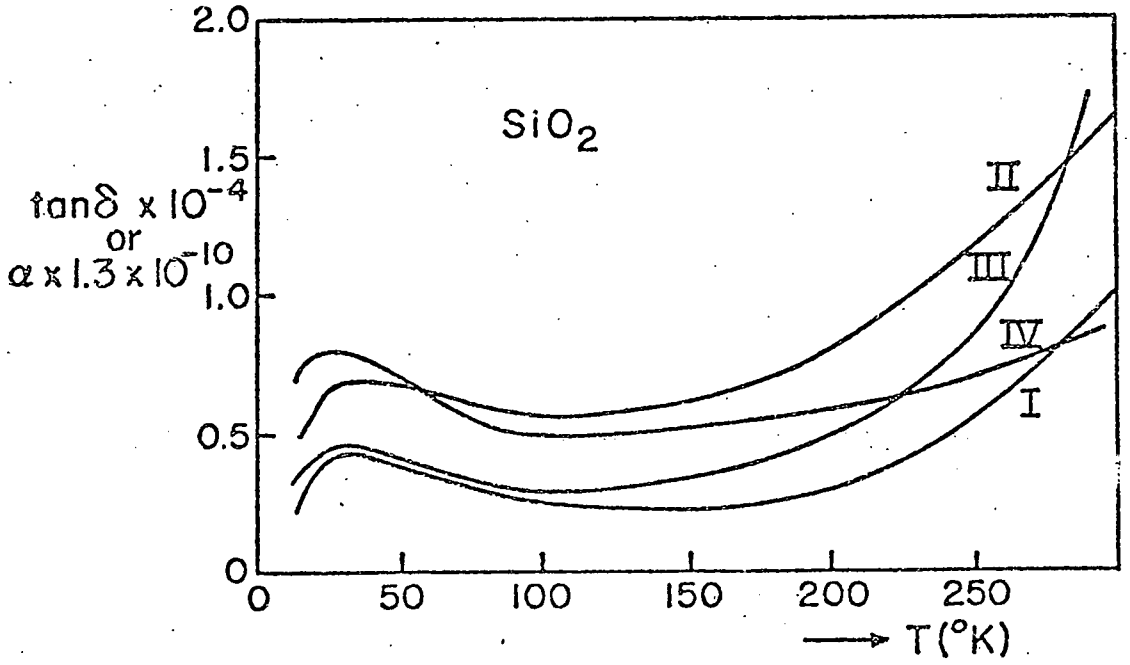

Figure 1.6b The absorption coefficient vs. temperature at 32 Kc/s for arbitrarily chosen specimens from four firms, after S. Volger and J.M. Stevels.[9] The four firms are British Thermal Syndicate (Curve I), Quartz et Silice (Curve II), Osram (Curve III), Heraeus (Curve IV).

reststrahlen region the temperature dependent absorption stems from higher order two-phonon processes. If cubic terms are present in the potential the absorption may occur in the following two ways: A photon is absorbed and two phonons are created (a summation process), or a photon is absorbed annihilating an existing phonon and creating another phonon (a difference process).

For an impure ordered crystal, in addition to optical mode transitions, the break down of the translational symmetry of the lattice causes almost all modes to become infrared active to some extent. The end result is that the lattice mode density of states is revealed as well as any local gap or resonant modes which are localized on this impurity and its neighbor.[14-16]

For glasses several theoretical models have recently been proposed to explain the frequency dependence of the absorptivity. One possibility is that the absorption arises from defect activated acoustic modes. Stolen[5] considers a model of an elastic, ordered solid to which a disordered charge distribution is added. For vitreous silica this disordered charge distribution could be due to defects such as an oxygen tetrahedron without a silicon centre, or an oxygen which is not bounded to two silicons. To arrive at an exact expression for the absorption coefficient Stolen uses the works of Schloman[17] and Vinogradov.[18] For small deviations of the ions the potential energy of an ideal lattice is given by:

$$U_o = U_o(0) + \tfrac{1}{2} \sum_{\substack{k\sigma \\ k\sigma'}} B_{kk'}^{\sigma\sigma'} b_k^{\sigma} b_{k'}^{\sigma'}$$

where K is the vector in the elementary cell; σ is a set of indices $\underline{s}$ and $\underline{x}$, where $\underline{s}$ is the number of ions in the cell and $\underline{x}$ denotes the component of the displacement along the $\underline{x}$-axis, and b_k^{σ} is the displacement of the ion and $B_{kk'}^{\sigma\sigma'}$ denotes the second derivative of the potential energy with respect to the displacement, evaluated at the equilibrium position of the ions. The equations of motion of the ions are: $m_s \ddot{b}_k^{\sigma} = -\partial U_o / \partial b_k^{\sigma}$ and we can represent the solution as a plane wave. Now consider a lattice with the potential energy $U = U_o + \delta U$, where δU is a nonperiodic term added to the potential because of the disordered charge distribution. Because of this term the ions will have new equilibrium positions and expanding the potential energy U in a series with respect to the displacement relative to the old equilibrium positions our new equations of motion are: $m_s \ddot{b}_k^{\sigma} + \sum_{k'\sigma'} (B_{kk'}^{\sigma\sigma'} + \delta B_{kk'}^{\sigma\sigma'}) b_{k'}^{\sigma'} - f_k^{\sigma} = (e_k^s + \delta e_k^s) E_k^{\sigma}$. Here f_k^{σ} denotes the negative derivative of the additional potential δU with respect to the displacement taken at the equilibrium position, and $\delta B_{kk'}^{\sigma\sigma'}$ is the second derivative of δU with respect to the displacements, taken at this same point: $e_k^s = e^s$ is the charge of ion $\underline{s}$ of the cell k; δe_k^s is the nonperiodic term added to the charge. The solution to the equations of motion are too long to be considered here and one is referred to Schlomann[17] and

Vinogradov[18] for a detailed solution. Vinogradov arrives at an expression for the imaginary part of the dielectric constant given by:

$$\epsilon_2 = \frac{2\overline{N(\delta e)^2}\omega}{\rho}\frac{1}{3}\left(\frac{2}{c_\tau^3} + \frac{1}{c_\ell^3}\right)$$

where N is the number of charges with contribute independently, δe is their charge, and ρ is the density of the sample. The imaginary part of the dielectric constant is related to the absorption coefficient by: $\alpha(\omega) = \omega\epsilon_2/c(2n)$ which gives an exact expression for the absorption coefficient

$$\alpha(\omega) = \frac{\overline{N(\delta e)^2}}{3\rho nc}\omega^2\left(\frac{2}{c_\tau^3} + \frac{1}{c_\ell^3}\right) \quad . \qquad (1.1)$$

The absorption should then be directly proportional to the frequency squared. To explain absorptions proportional to higher powers of the frequency one is required to assume some correlation among the defects. Such a correlation would exist if the defects in the neighbornood of a positive defect were more likely to be negative, creating neutral clusters.

Another model which attempts to explain the far infrared absorption of glasses has been proposed by P. W. Anderson[19] and W. A. Phillips.[20] The central hypothesis of their model is that there are tunneling states in amorphous solids; that in any glass there should exist a certain number of atoms (or groups of atoms) which can sit

more or less equally well in two equilibrium positions. They consider a particle in an asymmetric potential well as shown in the figure to the right. There are two minimas, separated by a barrier, which differ in energy by an amount 2Δ. Each isolated well has a set of wavefunctions ψ_1^n, ψ_2^n but they assume the

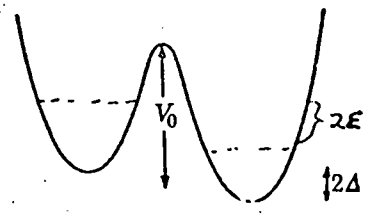

temperature sufficiently low for all states, but the ground state to have negligible probability of occupation. For a weakly coupled symmetric double well the wave functions are of the form $\psi_1 = 1/\sqrt{2}(\psi_1^0 + \psi_2^0)$, $\psi_2 = 1/\sqrt{2}(\psi_1^0 - \psi_2^0)$ with energies $\pm\Delta_0$. In general the well will not be symmetric and in particular an electric field $\vec{E}$ applied to the system introduces an asymmetry: the potential of one well is changed relative to the other by $\vec{\rho}_0 \cdot \vec{E}$, where $\vec{\rho}_0$ is the dipole moment when the particle is definitely in one well. For an asymmetry 2Δ the states have energies $\pm\varepsilon$ where $\varepsilon^2 = \Delta^2 + \Delta_0^2$, the particle is partly localized, leading to a resultant dipole moment of magnitude $\rho = \rho_0(\Delta/\varepsilon)$. The energies of the two states differ and in thermal equilibrium at a temperature T the average dipole moment is $\rho_0(\Delta/E)\tanh(\varepsilon/kT)$. Although each well has a dipole moment the average distribution makes the entire solid show no net polarization. The approach to

thermal equilibrium occurs with a relaxation time τ between states ψ_1 and ψ_2 with absorption or emission of a phonon of energy 2ϵ. Phillips[20] arrives at the real part of the dielectric constant over the different frequency regions given by:

$$\epsilon_o(0) - 1 = \frac{1}{\epsilon_o}\vec{\rho}_o\cdot\vec{E}\,\frac{\partial}{\partial\Delta}(\rho_o(\Delta/\epsilon))\tanh(\epsilon/kT)$$

$$\epsilon(\omega_1) - 1 = \frac{1}{\epsilon_o}\vec{\rho}_o\cdot\vec{E}\,\tanh(\epsilon/kT)\frac{\partial}{\partial\Delta}(\rho_o(\Delta/\epsilon)$$

$$\epsilon(\infty) - 1 = 0$$

where $1/\tau < \omega_1 < 2\epsilon/\hbar$ and where the region from $0 \leq \omega \leq \omega_1$ corresponds to relaxation absorption and the region from $\omega_1 \leq \omega < \infty$ corresponds to resonant absorption (see Figure 1.7). π the imaginary part of the dielectric constant is related to the real part by the Kramers-Kronig equations which give:

$$\int_{\omega_1}^{\infty}\frac{\epsilon''(\omega)}{\omega}d\omega = \frac{\pi}{2}(\epsilon(\omega_1) - \epsilon(\infty)) = \frac{\pi}{2\epsilon_o}\vec{\rho}_o\cdot\vec{E}\rho_o\,\tanh(\epsilon/kT)\frac{\partial}{\partial\Delta}(\Delta/\epsilon)$$

We now have that the area under the resonant absorption divided by the frequency squared curve is:

$$\int\frac{\alpha}{\omega^2}d\omega = \frac{\pi}{2\epsilon_o}\vec{\rho}_o\cdot\vec{E}\frac{\rho_o\tanh}{2nc}(\epsilon/kT)\frac{\partial}{\partial\Delta}(\Delta/\epsilon) \quad . \qquad (1.2)$$

Whenever we have a tunneling mode we should then expect that at low temperatures the area under the $\alpha(\omega)/\omega^2$ curve should go as $\tanh(\epsilon/kT)$ where 2ϵ is equal to the energy of the absorbed phonon (i.e. $\epsilon = \hbar\omega_o/2$, where ω_o is the

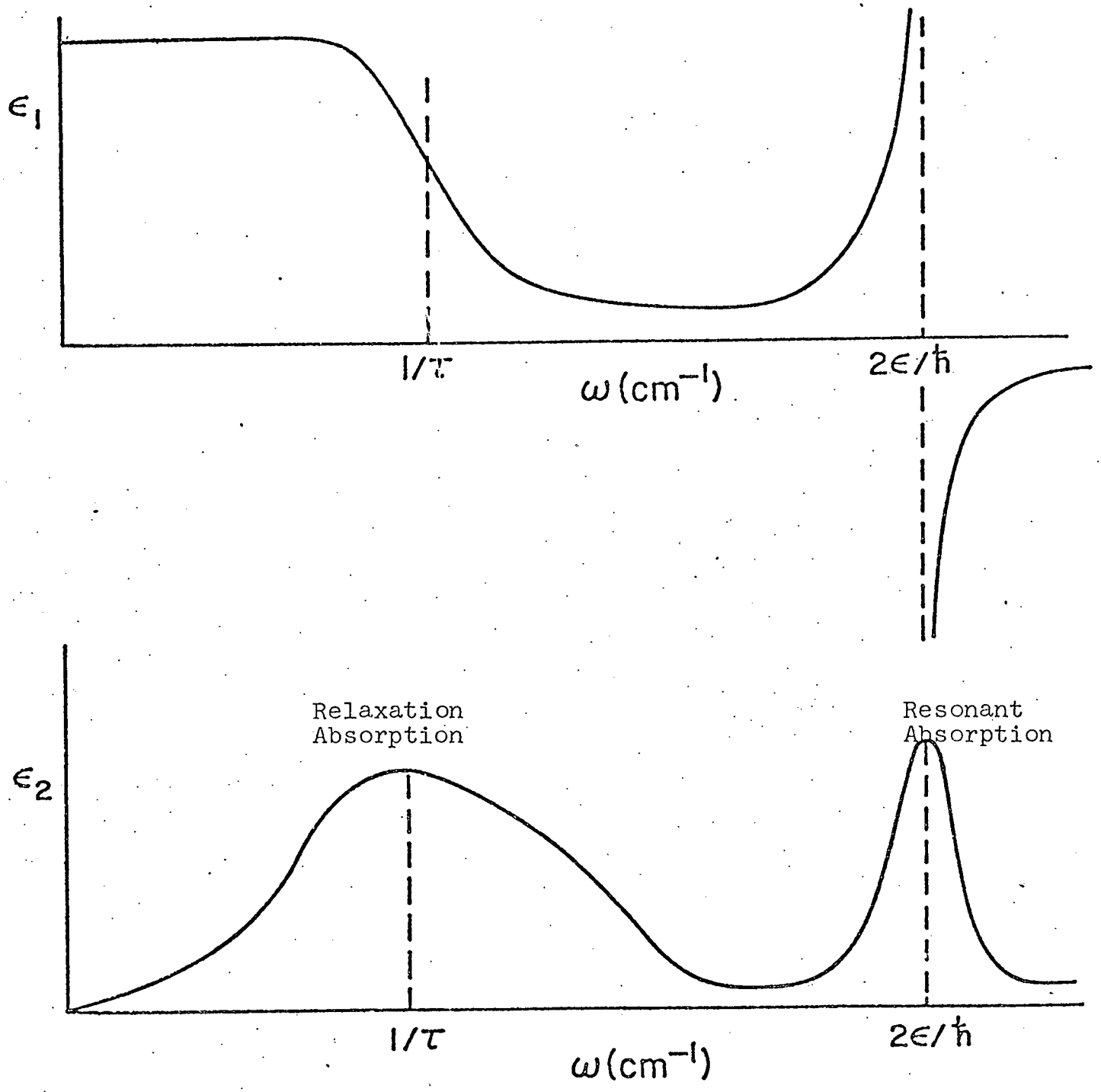

Figure 1.7 The real (ϵ_1) and the imaginary (ϵ_2) parts of the dielectric constant vs. frequency. The region near $1/\tau$ corresponds to relaxation absorption and the region near $2\epsilon/\hbar$ corresponds to resonant absorption.

frequency at which the tunneling mode occurs).

The last model which we consider has been proposed by E. Wallay.[7] His theory is based on certain assumptions which are: (1) The glass is composed of units A, which might be atomic or molecular, arranged in an irregular glass-like manner; (2) The potential energy U can be written as the sum of square terms in the internal coordinates $s(\ell,k)$, $U = \frac{1}{2}\sum_{\ell,k} \varphi(k)s^2(\ell,k)$ where k identifies the kind of internal coordinate and ℓ identifies the particular unit of the k^{th} internal coordinate. For the potential to be written as given it is important that the internal coordinates be chosen so that the potential energy contains no cross terms in the internal coordinates. (3) The glass has a dipole moment which is linear in the interval coordinates. The dipole moment derivatives are $M(\ell,k) = \partial u/\partial s(\ell,k)$, where u is the dipole moment. It is also assumed that there is no correlation among the values of $M(\ell,k)$ for neighboring coordinates. The solid has no net polarization so the mean value of $M(\ell,k)$ averaged over all ℓ is zero. (4) The quantity $M^2(\ell,k)$ occurs only in sums like $\sum_{\ell,k} M = (\ell,k)\left\{\frac{\partial s(\ell,k}{\partial Q_k}\right\}$. And that there is little correlation between the mechanical and the electrical properties of the crystal, so that for any vibration the above sum can be replaced by:

$$\sum_k \langle M^2(\ell,k)\rangle_\ell \sum_\ell \left\{\frac{\partial s(\ell,k)}{\partial Q_k}\right\}^2$$

where $\langle\rangle_{\ell}$ means the average over all ℓ. It is further assumed that this average is independent of the particular vibration. Whalley expects this to be true in the acoustic branches but not in general for the vibrations associated with defects in the glass structure such as broken bonds. From these assumptions Whalley arrives at a formula for the absorption coefficient given by:

$$\alpha(\omega) = \frac{1}{n}\left(\frac{n^2+2}{3}\right)^2 \frac{\pi^2}{3c} R\omega^2 g(\omega) \qquad (1.3)$$

where n is the refractive index at frequency ω, c the speed of light, R is the effective dipole moment derivative, and $g(\omega)$ is the density of vibrational states per unit volume.

The three models which attempt to explain the far infrared absorption in glasses show that the important thing to consider is not the absorptivity but the absorptivity divided by the frequency squared. The first model, equation (1), predicts that the $\alpha(\omega)/\omega^2$ vs. ω curve should be constant; the second model, equation (2) predicts that the area under this curve at frequencies where modes exist should go as the $\tanh(\hbar\omega/2kT)$; the third model, equation (3), predicts that the $\alpha(\omega)/\omega^2$ curve should be closely related to the density of states. Our data will be presented in this form (Chapter III) so that some comparison can be made to the various theoretical models.

In Chapter II, we will discuss the far infrared techniques and apparatus with emphasis on how we measured the

absolute value of the absorption coefficient. Chapter IV will be to compare our data to: (1) measurements done by other researchers on the same glasses, (2) measurements done on other glasses, and (3) the absorption predicted by the various models presented here.

CHAPTER II

FAR INFRARED TECHNIQUES AND APPARATUS

A. Introduction

The far-infrared is characterized by frequencies between microwaves and infrared. This is considered to be in the range from 2 cm^{-1} to 200 cm^{-1}. Frequencies are given in terms of wave numbers (cm^{-1}) but these can easily be converted into other units of energy by the following relations: 1 cm^{-1} = 30 GHz = 0.124 meV = 1.44°K = 1.88 x 10^{-12} ergs.

The source of the far-infrared radiation is the black body radiation from a mercury arc. The spectrum is analyzed by Fourier transform spectroscopic techniques which employ either a Michelson or a lamellar-grating interferometer. An interferometer produces an interferogram by the superposition of two coherent light beams as a function of their optical path difference. The interferogram is recorded in terms of the intensity vs. the distance distribution and by Fourier analyses converted into an intensity vs. frequency distribution. The Michelson interferometer will be described briefly. A complete description of the lamellar is given by Kirby,[21] Lytle,[22] and Sievers.[23]

B. Michelson Interferometer

A schematic diagram of a Michelson interferometer is shown at right. The light from the source is divided by the beam splitter into Beams I and II. Each beam is then reflected at Mirrors I and II and divided again at the beam splitter. We are only interested in the parts of Beams I and II which overlap and form Beam III, traveling toward the detector. Let us first consider a monochromatic source with the distance from the beam splitter to the Mirrors to be the same ($x = 0$). Then there is no phase difference between Beams I and II, when they recombine they interfere constructively and the signal at the detector is a maximum. Now move Mirror II a distance $x/2$, still with a monochromatic source. The superposition of the two beams can now be expressed as $g(x) = 2A\,(1 + \cos(2\pi\omega_o x))$ where A is the amplitude of the equal fractions of Beams I and II and ω_o is the frequency of the monochromatic light and x is the path difference. For $x = 0, \lambda, 2\lambda \ldots$ we will get a maximum signal at the detector and for $x = \lambda/2,\ 3\lambda/2 \ldots$ we will get a minima.

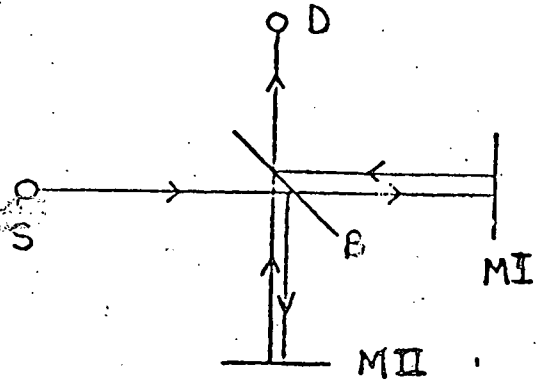

Figure 2.1
Michelson Interferometer

Now we will consider a source that emits light of a continuous spectrum of frequencies $0 \leq \omega \leq \infty$. The

amplitude A becomes a function of ω and we have to integrate from $\nu = 0$ to $\omega \to \infty$.

$$g(x) = \int_0^\infty 2A(\omega)(1 + \cos(2\pi\omega x)d\omega$$

$$= \int_0^\infty 2A(\omega)d\omega + \int_0^\infty 2A(\omega)\cos(2\pi\omega x)d\omega$$

for $x = 0$ we have: $g(0) = \int_0^\infty 2A(\omega)d\omega + \int_0^\infty 2A(\omega)d\omega = 2\int_0^\infty 2A(\omega)d\omega$. We can now rewrite our equation as:

$$s(x) = g(x) - g(0)/2 = \int_0^\infty 2A(\omega)\cos(2\pi\omega x)dx$$

where $s(x)$ is the interferogram function; intensity as a function of distance (mentioned in introduction). Figure 2.2a shows a diagram of either $s(x)$ or $g(x)$. Taking $A(\omega)$ to be an even function we can rewrite $s(x)$ as:

$$s(x) = \int_{-\infty}^\infty A(\omega)\cos(2\pi\omega x)d\omega$$

and its Fourier transform as: $A(\omega) = \int_{-\infty}^\infty s(x)\cos(2\pi\omega x)dx$ $= \int_{-\infty}^\infty [g(x) - \frac{1}{2}g(0)]\cos(2\pi\omega x)dx$. We have therefore arrived at our desired result, an intensity vs. frequency spectrum (Figure 2.2b). The $g(x)$'s are fed directly to an online computer as x is stepped from zero to x_{max} in increments on Δx. Stopping x at a finite value introduces errors which determine our resolution. This is described in more detail by Nolt.[24]

Figure 2.3 shows a schematic diagram of the data acquisition system. The signal from the detector is

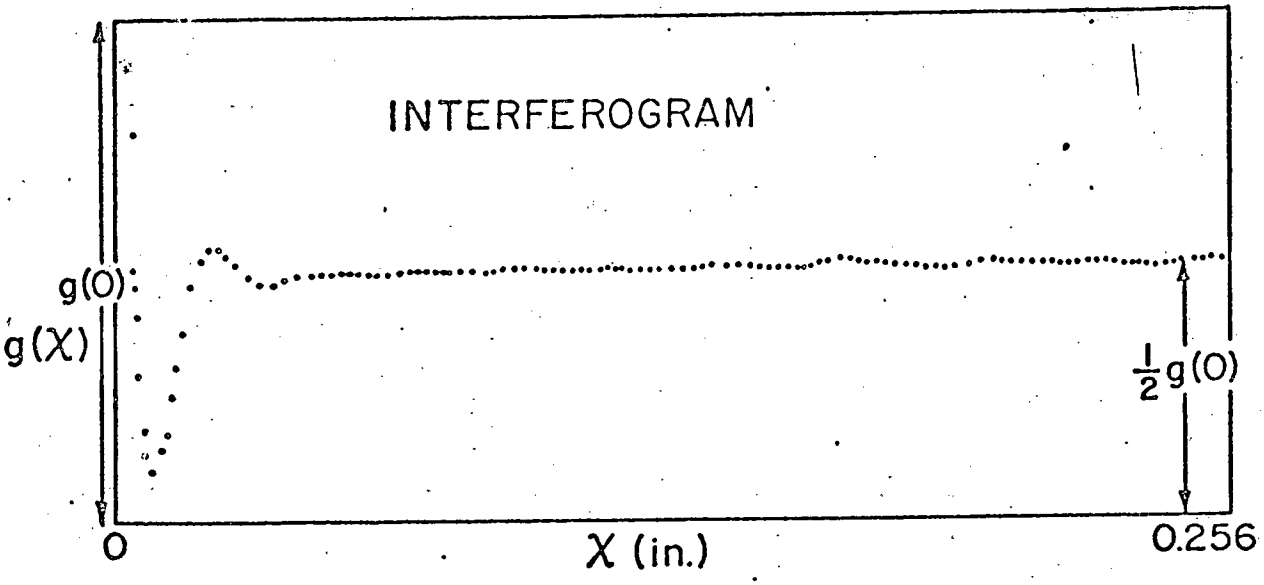

Figure 2.2a

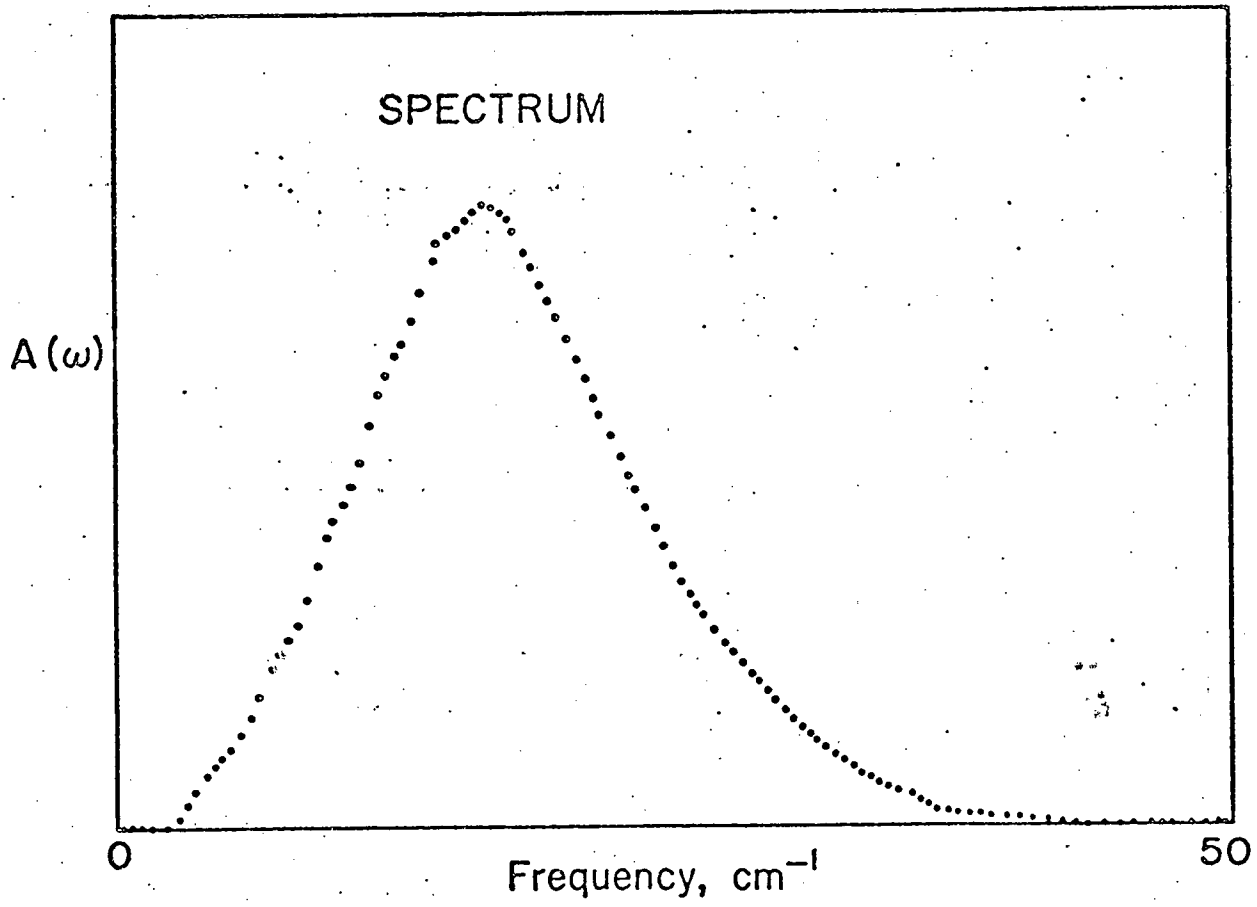

Figure 2.2b

Figure 2.2 Interferogram and spectrum for a 2 cm. long sample of vitreous silica.

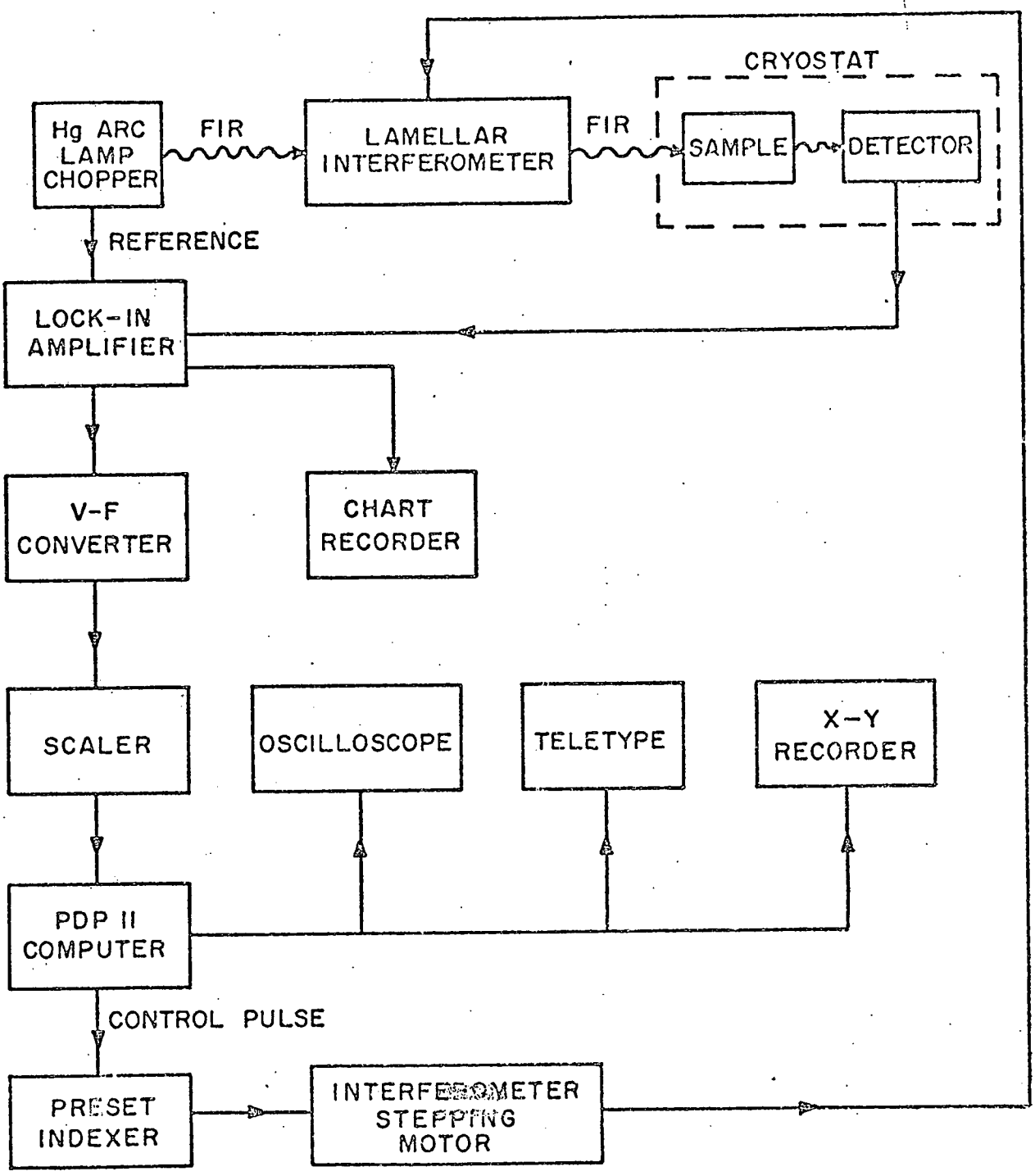

Figure 2.3 Schematic diagram of the data acquisition system.

amplified, digitized and is then sent on line to a PDP-11 computer.[25] Using a program written by H. Ziegler, the computer immediately Fourier transforms a given number of points and continuously displays the interferogram, the spectrum, ratio, or absorption to a previously obtained spectrum on the oscilloscope. The computer controls the stepping, has noise discrimination capability and can average consecutive runs.

C. Cryostat

The cryostat used for all measurements was designed, built and described by D. Tanner.[26] We will give a brief description here. The apparatus is shown diagramatically in Figure 2.4. The cryostat is surrounded by glass liquid helium and liquid nitrogen dewars. Going from top to bottom we have the radiation going down a 1/2" i.d. brass light pipe to the samples which are contained in a sample rotator. The sample rotator allows us to use up to 5 samples for each run. After going through the sample, the radiation then goes through two quartz vacuum windows, and through a section surrounded by a He^4 pot. This pot is connected to an outside pump and is filled from the outer bath by a needle valve; after which the He^4 inside is pumped to a temperature of about 1^oK. The radiation then goes through a condensing cone which increases the maximum angle that it makes with the axis of the light pipe from 18^o to 90^o. The radiation then enters the

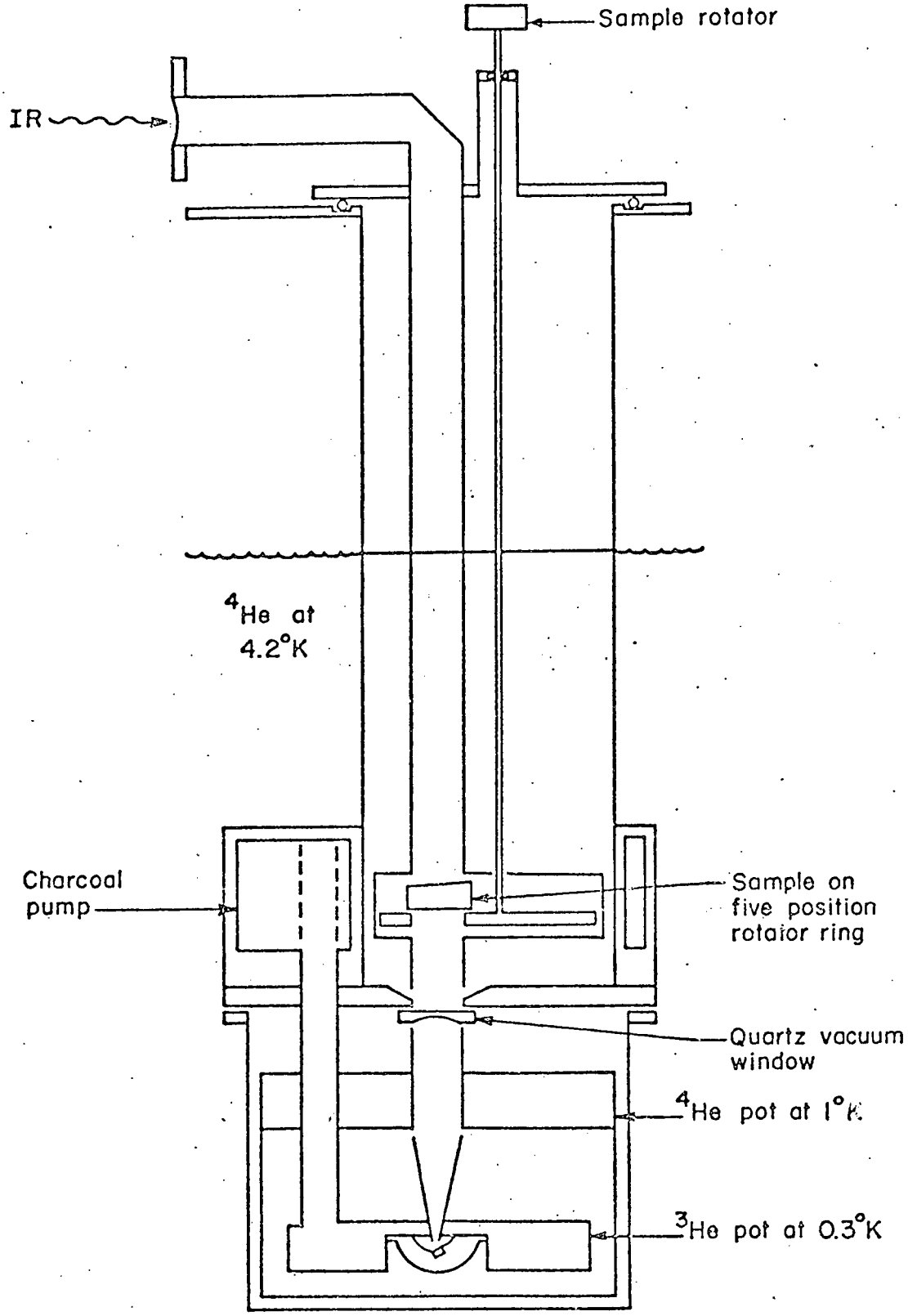

Figure 2.4 Sketch of detector cryostat. Glass liquid helium and liquid nitrogen dewars surround the cryostat.

hemispherical integrating cavity where a germanium detector sits. This cavity is surrounded by a He^3 pot. This pot is connected to a charcoal pump which is located in a vacuum can just above the detector section. When the charcoal is cooled (by filling the vacuum section around the charcoal section) it pumps the He^3 to a temperature of about $0.3^{\circ}K$.

The operation of the cryostat is as follows: The night before a run we pump out the glass dewar double wall section and leave an air pressure of about 200 microns; pump out the charcoal vacuum insulation; pump out the helium, sample and detector sections and backfill them with an atmosphere of helium gas; fill the liquid nitrogen dewar. Next day, refill the liquid nitrogen dewar and re-backfill the helium and sample sections with an atmosphere of helium gas. Check to see that everything is at liquid nitrogen temperature and begin transferring liquid helium. Once the level of the liquid helium is above the needle valve the $1^{\circ}K$ pot is filled and pumped down. Since the charcoal is isolated from the outer bath it is still at liquid nitrogen temperature and the He^3 will condense against the $1^{\circ}K$ pot and drip down into the pot surrounding the detector. This takes about 20 minutes and after checking to see that the He^3 and the He^4 are at $1^{\circ}K$ one is ready to pump on the He^3. This is done by letting a pinch of helium gas into the vacuum can surrounding the charcoal. The charcoal cools down and at

about 20°K it begins to pump on the He^3. The He^3 is pumped down to about 0.3°K very quickly and the dewar is refilled with sufficient liquid helium. We again refill the 1° pot and we are now ready to take data.

D. Measuring the Absorptivity

To arrive at an exact expression for the intensity going through a sample of length d, one must include the effect of multiple reflections within the sample. Figure 2.5 illustrates how multiple reflections can occur in a sample with flat faces. In order to determine the resulting amplitude of the entire emerging beam and hence the total transmitted intensity, it is necessary to sum over the amplitudes and phases of all the emerging rays. The phase difference between two successive rays emerging from the glass is $\Delta\varphi = 2\pi/\lambda \cdot 2d$. Which becomes $\Delta\varphi = 4\pi n\omega d$, where ω is in cm^{-1} and c = 1 and n is the refractive index. We can now add all the amplitudes, which give the following infinite series:

$$A_t = A_o*(1-R)*e^{-\alpha d/2}(1 + R*d^{-\alpha d}*e^{i\Delta\varphi} + R^2*e^{-2\alpha d}*e^{2i\Delta\varphi} + \ldots)$$

where A_o is the amplitude of the incident radiation, α is the absorption coefficient and R is the reflection from a single surface: $R = (n-1)^2/(n+1)^2$. This geometric infinite series is easily solved to give the resultant transmitted amplitude:

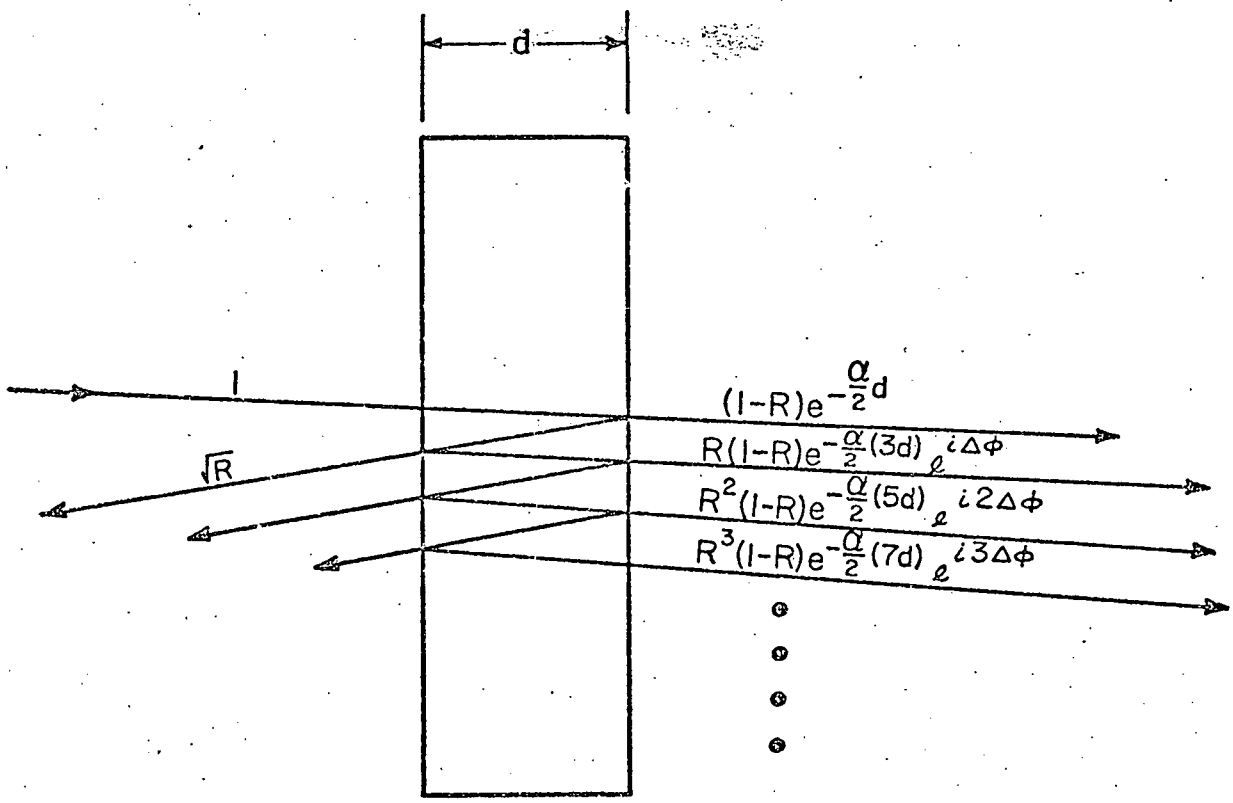

Figure 2.5 Multiple reflections within a glass slab.

$$A_t = A_o \frac{(1 - R)*e^{-\alpha d/2}}{1 - R*e^{-\alpha d}e^{i\Delta\varphi}} \quad .$$

Which gives a transmitted intensity spectrum of:

$$I(\omega) = \frac{I_o(\omega)(1-R)^2*e^{-\alpha d}}{1+R^2*e^{-2\alpha d}-2R*e^{-\alpha d}} \cos(4\pi\omega dn) \qquad (2.1)$$

where $I_o(\omega)$ is the intensity spectrum of the incident beam. To calculate the absorption coefficient from equation 2.1 one must know the incident intensity as a function of the frequency, the transmitted intensity as a function of the frequency and the index of refraction as a function of the frequency. Our apparatus is capable of measuring $I(\omega)$ and $I_o(\omega)$ but not $n(\omega)$. It would therefore be a great advantage if we could calculate the absorption coefficient without having to know the index of refraction.

Not considering the multiple reflections within the sample one would arrive at a transmitted intensity spectrum given by

$$I(\nu) = I_o(\omega)(1-R)^2*e^{-\alpha d} \quad . \qquad (2.2)$$

Although this equation also includes the index of refraction, it can be eliminated by taking the ratio of the transmitted intensities of two samples of different lengths. The absorption coefficient would then be equal to the natural log of this ratio divided by the difference in the sample lengths

$$\alpha = \ell n(I_2/I_1)/(d_1-d_2)$$

which does not involve knowing the index of refraction. The difference between equations 2.2 and 2.1 is seen to be $1 + R^{2*}e^{-2\alpha d} - 2R^{*}e^{-\alpha d}\cos(4\pi\nu dn)$. Let us first see how large this effect is and then how we can eliminate it. For vitreous silica the value of the index of refraction is $n = 1.95$,[27] which gives a value of $R = 0.1$. The maximum value of $R^{2*}e^{-2\alpha d}$ is then 0.01 and the value of $2R^{*}e^{-\alpha d}\cos(\theta)$ oscillates from -0.2 to +0.2. We arrive at a maximum error of 21% by using equation 2.2 instead of equation 2.1. The easiest way to reduce this discrepancy is to use longer samples. For our quartz samples we used various lengths such that the value of αd was always greater than 0.5. This would make the second term in the correction factor negligible. The third term would oscillate from -0.1 to +0.1. Using these lengths our error would be less than ±10%. This error is still significant so to further reduce it we rounded the flat faces of our samples to at least 2 mm. Appendix A shows how a non-flat face would eliminate multiple reflections making the use of equation 2.1 not necessary.

Another effect which we had to consider was the internal reflections off the sides of our samples. The Figure on the next page shows how an incident angle different from zero will result in some internal reflections. The transmission through the sample is given by: $T = e^{-\alpha_e L}$,

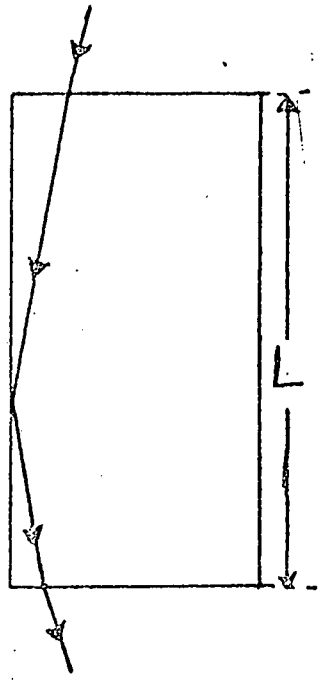

where α_e is the measured absorption coefficient in the light pipe. Because of these internal reflections $\alpha_e L = \alpha L_{eff}$, where α is the real absorption coefficient and L_{eff} is the effective length given by: $L_{eff} = L(1 + \epsilon_1 L + \epsilon_2 L + \ldots)$ with ϵ_1, ϵ_2, ϵ_3,... = correction factors. Then $L_{eff} L = (1 + \epsilon_1 L + \epsilon_2 L^2 + \ldots)$ and $\alpha_e = \alpha \frac{L_{eff}}{L}$. Now we have $\alpha_e = \alpha \cdot (1 + \epsilon_1 L + \epsilon_2 L^2 + \ldots)$. In practice we measure the absorption coefficient by taking the difference of two lengths, therefore $\alpha_e = \alpha(1 + \epsilon_1 \Delta L + \epsilon_2 \Delta L^2 + \ldots)$. Now when $\Delta L \rightarrow 0$, $\alpha_e \rightarrow \alpha$. To arrive at the real absorption coefficient we graph the effective absorption coefficient as a function of ΔL (the difference in length between samples). For four samples in the sample rotator this would give six points on the graph (i.e. L_4-L_1, L_3-L_1, L_2-L_1, L_4-L_2, L_3-L_2, L_4-L_3). These points are connected by a straight line (see Figure 2.6), which is extrapolated to zero difference to give the real absorption coefficient.

One problem we came across was that at low frequencies (below 15 cm^{-1}) we were getting as much transmission through the long samples as through the shorter samples when we used samples which were 3/8" diameter. When we switched to 1/2" diameter samples this effect disappeared. This effect

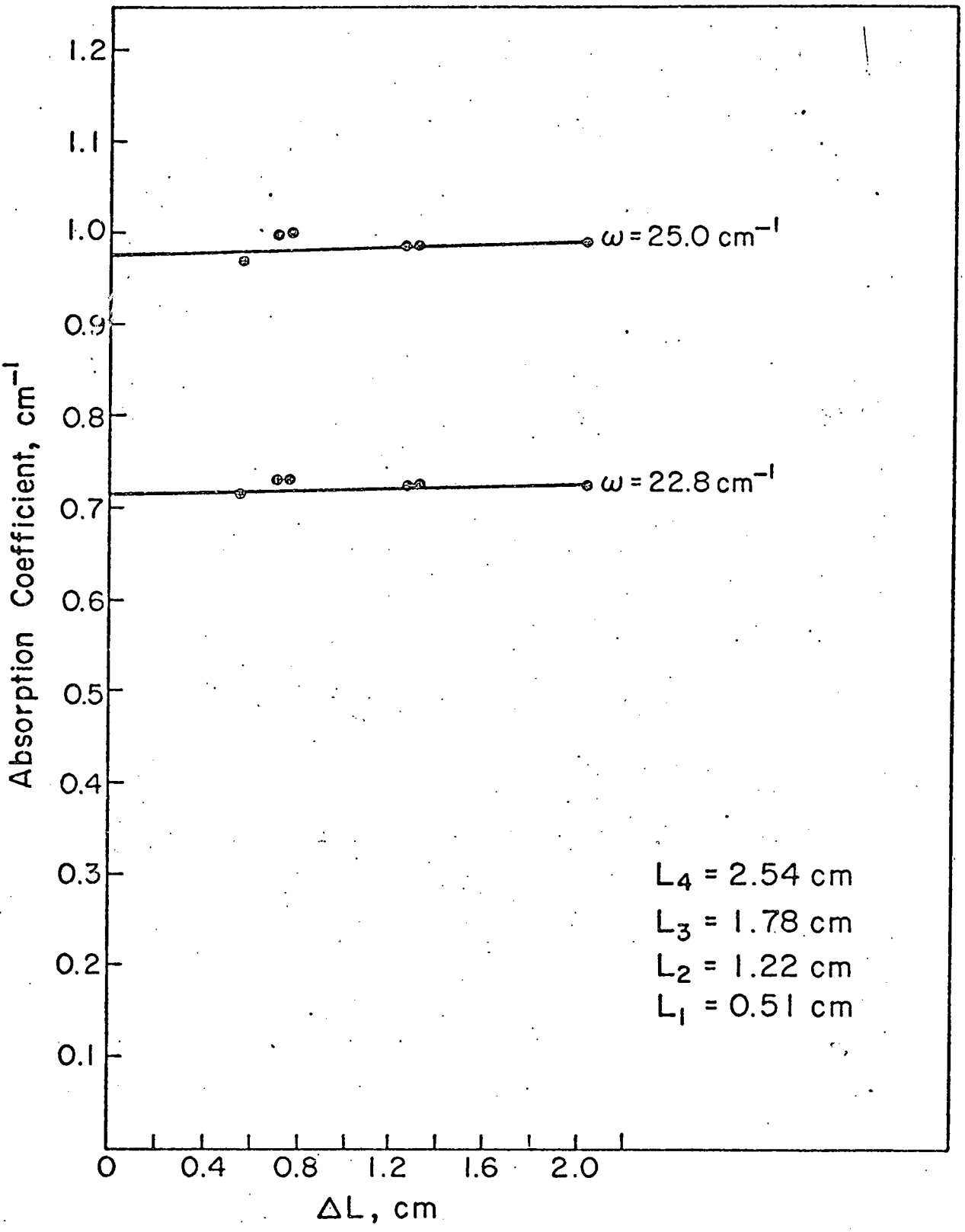

Figure 2.6 The absorption coefficient vs. difference in length at 25 cm^{-1} and 22.8 cm^{-1}. The four sample lengths are 2.54 cm., 1.78 cm., 1.22 cm., and 0.51 cm.

could occur if the absorption of a 3/8" i.d. brass light pipe is the same order of magnitude as that of fused quartz. This can be shown by letting the absorption coefficient of the quartz and the light pipe be α_1 and α_2. Then the transmission is

$T \alpha \exp.(-\alpha \ell_1 - \alpha \ell_2)$ where ℓ_1 = length of quartz;

ℓ_2 = length of 3/8" light pipe

and $\ell_1 + \ell_2 = \ell$ constant length of sample holder. Which becomes $T \alpha \exp.(-(\alpha_1 - \alpha)\ell_1 - \alpha_2 \ell)$ and if $\alpha_1 = \alpha_2$ we have $T \exp.(-\alpha_2 \ell)$ or the transmission is independent of the length of the sample. Does the absorption of a 3/8" light pipe have the same order of magnitude as quartz?

Using the theoretical and experimental data of Richards[28,29] on the transmission of brass light pipes, we arrived at an absorption of about 0.007 cm^{-1} at a frequency of 10 cm^{-1}. The absorption of quartz at this frequency (from our data) is 0.066 cm^{-1} or one order of magnitude higher than that of the light pipe. The absorption of the light pipe is therefore a large effect at small frequencies but not large enough to explain what occurred with our 3/8" samples. This discrepancy remains a puzzle.

E. Samples.

All samples used were in cylindrical rods. At first samples with a diameter of 3/8" were used, but these resulted in some problems (see previous section) and for

the measurements reported here samples of 1/2" diameter were used. The vitreous silica samples were obtained both from the glass shop at Cornell and also from Valpey Corp.[30] There was no noticeable difference in the absorption spectrum between these different samples. The samples from the Valpey Corp. were G.E. 125 which contained no water. The concentration of impurities was less than 200 ppm. with the largest impurity being Al_2O_3.

The GeO_2 samples were grown at the Cornell crystal growing facilities by heating germanium powder continuously in a vacuum for 24 hours until it reached a temperature of 1100°C. Then introducing slightly less than an atmosphere of oxygen for 6 hours at 1200°C. Then letting the glass cool slowly.

The $CaK(NO_3)_3$ was produced from equimolar amounts of AR grade KNO_3, and $Ca(NO_3)_2 \cdot 4H_2O$.[31] It was heated by a bunsen burner in air in a pyrex beaker until the mixture dissolved into its own water of hydration. It boiled until a white precipitate formed which redissolved upon further heating. One can not heat the material much beyond this point since the NO_3^- starts to break down with the emission of brown fumes. We heated the mixture for a couple of minutes after the precipitate had dissolved and then poured it into a clean hot test tube. It is hard to avoid nucleation centers so about 1/3 of the sample would crystallize, but these can be reheated. Since $CaK(NO_3)_3$ is very hygroscopic it was left to cool, at

room temperature, in a bell jar. During cooling the glass contracts and breaks the pyrex test tube, and we are left with cylindrical rods.

CHAPTER III

EXPERIMENTAL DATA

A. Introduction

In this Chapter all of our data will be presented. We have measured the far infrared absorption coefficient of three glasses; two of which are very similar in chemical structure (SiO_2 and GeO_2) and the other ($CaK(NO_3)_3$), an ionic glass, has a completely different chemical structure. Our data is given in the form of $\alpha(\omega)/\omega^2$ vs. ω to comply with the various theoretical models discussed in Chapter I. Before discussing our measurements of the absorption curves of the various glasses we will compare our measurements of a disordered ionic crystal to that of a glass. Figure 3.1 shows our measurements of the far infrared absorption spectrum of $KCl_{20\%}$:$KBr_{80\%}$ and vitreous silica. The crystal shows an absorption coefficient which is constant over our range of frequencies, which was surprising since we expected a frequency squared dependence (see equation 1.1). The glass on the other hand shows a very definite frequency dependence. We can see from Figure 3.1 that the far infrared absorption of the disordered ionic crystal ($KCl_{20\%}$:$KBr_{80\%}$) and the glass (SiO_2) are in no way similar.

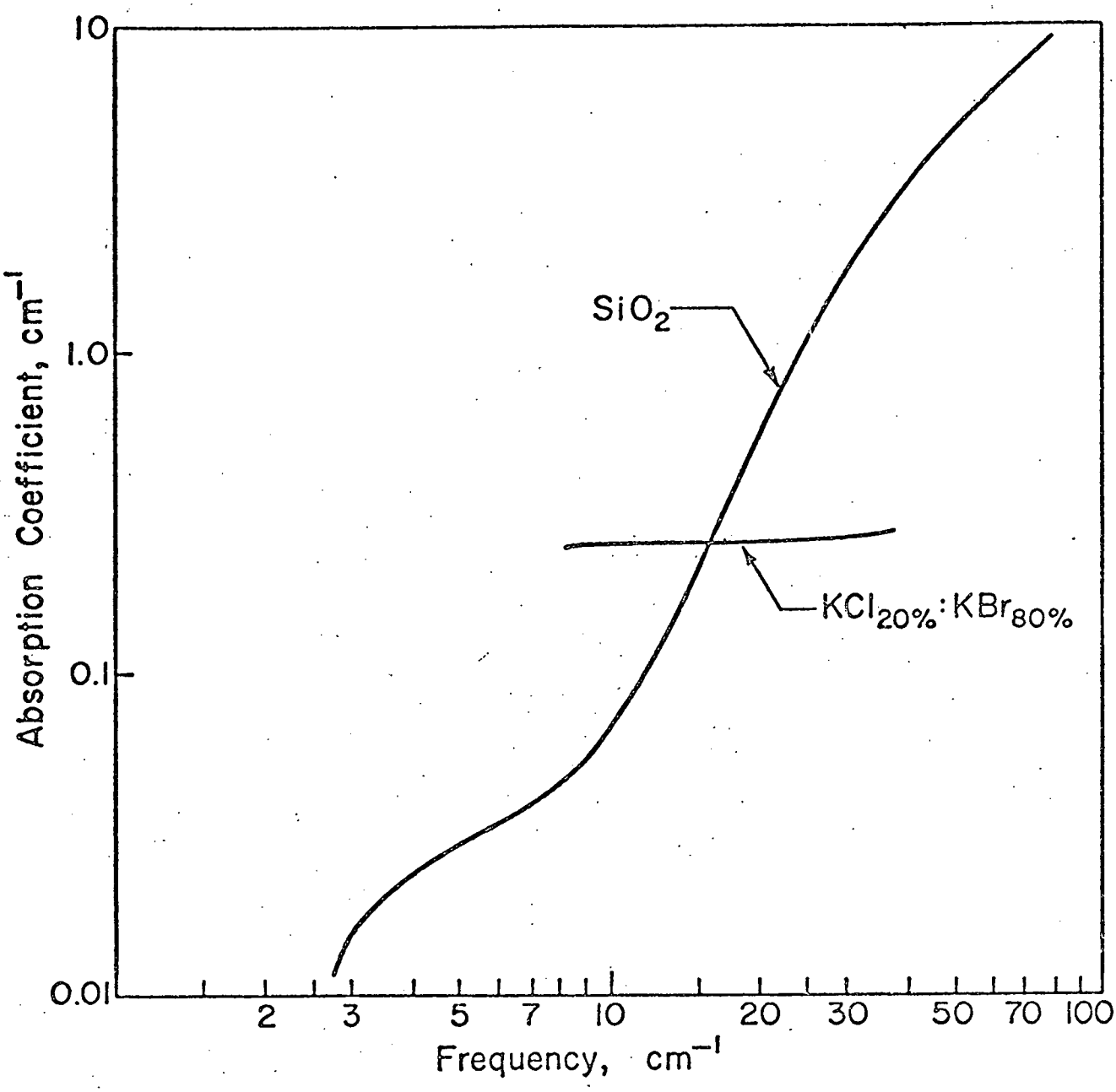

Figure 3.1 The absorption coefficient vs. frequency for $KCl_{20\%}$:$KBr_{80\%}$ and vitreous SiO_2.

B. Absorption Coefficients

Figure 3.2 shows the graph of the absorption coefficient divided by the frequency squared ($\alpha(\omega)/\omega^2$) versus the frequency for vitreous silica in the range from 2 cm^{-1} to 78 cm^{-1} at 4.2°K. The point at 1 cm^{-1} comes from the dielectric loss measurements made by E. M. Amrhein. There is a peak in our graph at 40 cm^{-1}, similar to other works which have shown peaks at 38 cm^{-1} [7] and 42 cm^{-1}.[6] Our data also show another peak at 3.0 cm^{-1} where other researchers had not been able to extend their results. Although we have been the first to measure this peak, it had been suggested by Whalley[7] from the density of states derived from heat capacity measurements. These measurements show that the heat capacity divided by the temperature cubed falls with decreasing temperature down to about 2°K[32] but then increases between that temperature and 0.64°K.[33,34] From these measurements Whalley expects there to be a maximum in the density of states at a few cm^{-1}. Recent measurements[1] though, show that the density of states from the specific heat increases steadily to at least 0.13°K and is expected to increase linearly with decreasing temperature. There is therefore no peak in the density of states at a few cm^{-1}.

Figure 3.3 shows our measurements on GeO_2 from 10 cm^{-1} to 40 cm^{-1} at 4.2°K. There is a peak in $\alpha(\omega)/\omega^2$ at 34 cm^{-1}, similar to that reported by Stolen[6] at 38 cm^{-1}.

Figure 3.2 The absorption coefficient of vitreous SiO_2 plotted as $\alpha(\omega)/\omega^2$ vs. ω.

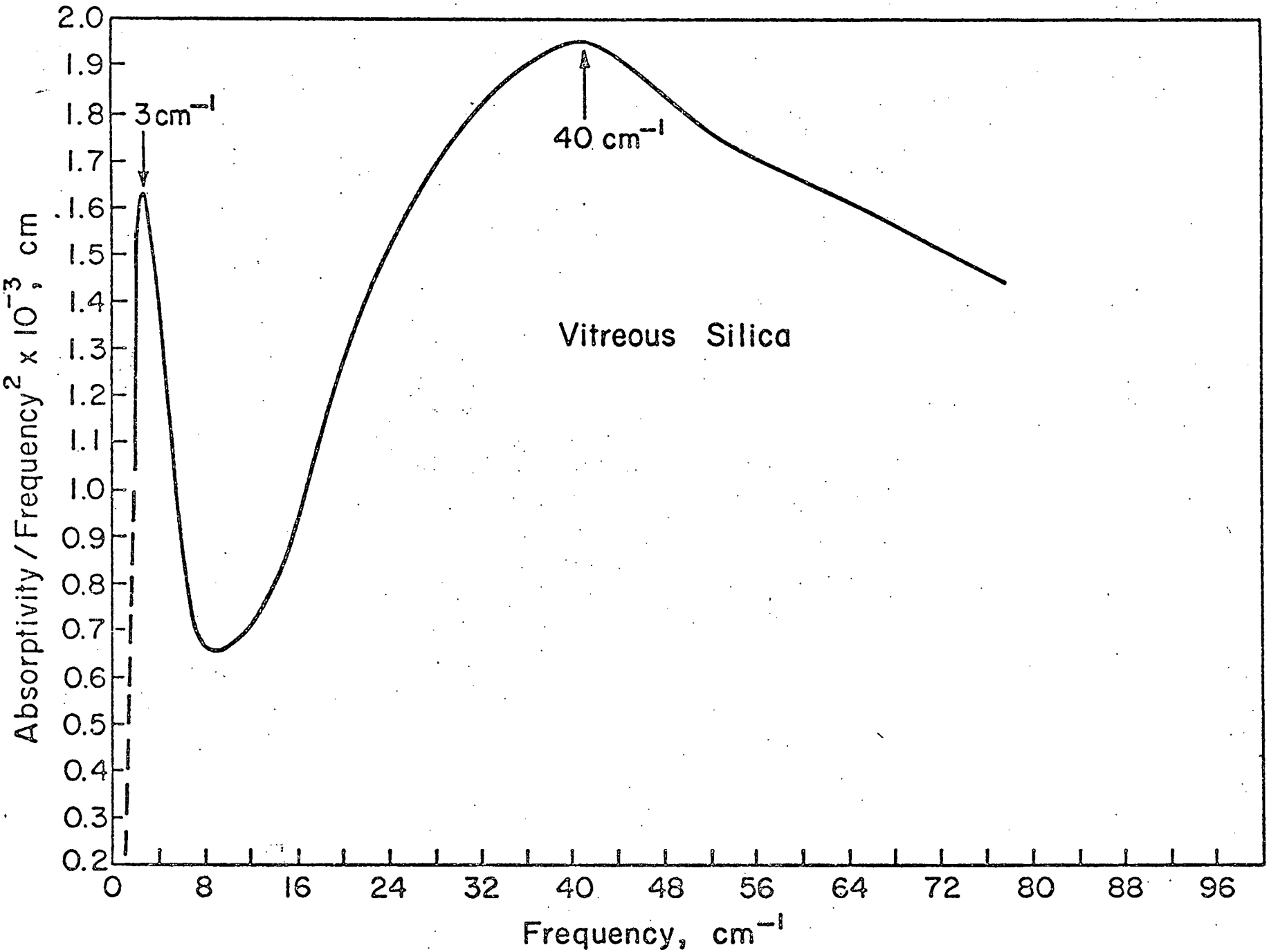
3 cm⁻¹
40 cm⁻¹
Vitreous Silica
Absorptivity / Frequency² x 10⁻³, cm
Frequency, cm⁻¹
2.0
1.9
1.8
1.7
1.6
1.5
1.4
1.3
1.2
1.1
1.0
0.9
0.8
0.7
0.6
0.5
0.4
0.3
0.2
0
8
16
24
32
40
48
56
64
72
80
88
96

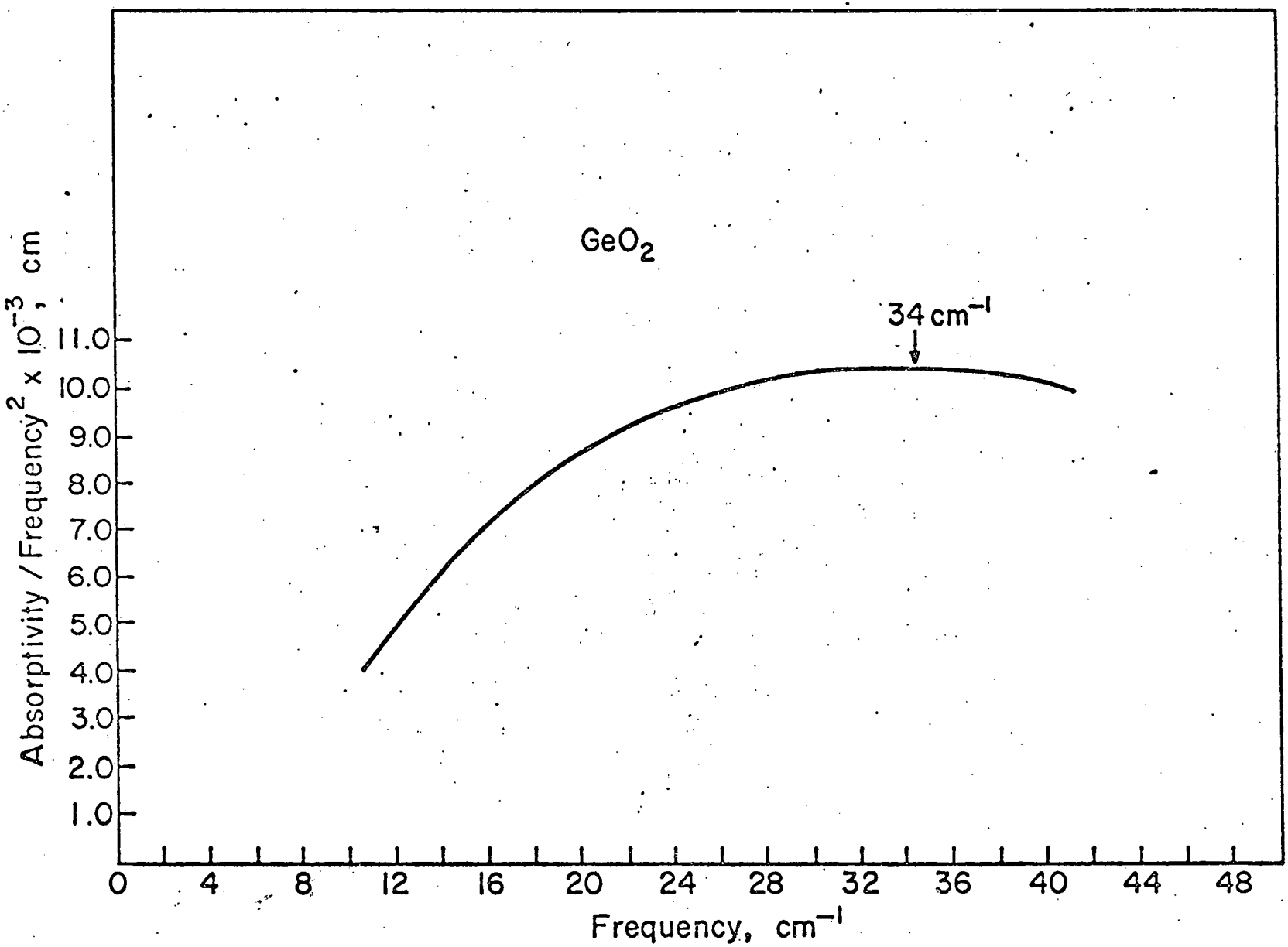

Figure 3.3 The absorption coefficient of vitreous GeO_2 plotted as $\alpha(\omega)/\omega^2$ vs. ω.

Qualitatively the absorption spectra of the two glasses are very similar even though their absolute magnitudes differ.

Our measurements for the ionic glass, $CaK(NO_3)_3$, are shown in Figure 3.4. We have measured its absorption from 3 cm^{-1} to 18 cm^{-1} at 4.2°K. We measured a peak in $\alpha(\omega)/\omega^2$ at 3.8 cm^{-1}. No previous measurements have been made on this type of glass.

C. Temperature Dependence of the Absorptivity

Our measurements on the absorption of the various glasses show some low lying modes. If these were caused by low energy tunneling states there would be a strong temperature dependence of the absorption at the frequencies where these states occur. At other frequencies there would be little change with temperature. Our measurements of the temperature dependence of vitreous silica tend to disprove the tunneling model. For vitreous silica we measured an anomoly at 3.0 cm^{-1}. The energy difference between the tunneling states would then be on the order of 2.8 cm^{-1} or 4.0°K. Then according to Phillips[20] (equation 1.2) the factor $\tanh(\hbar\omega/2kT)$ represents the increase in the absorption with decrease in temperature because of the change in the relative populations of the two levels. To see if this mode is due to tunneling states we measured the transmission through a 5.1 cm long sample of SiO_2 at 4.2°K and at 1.0°K. A

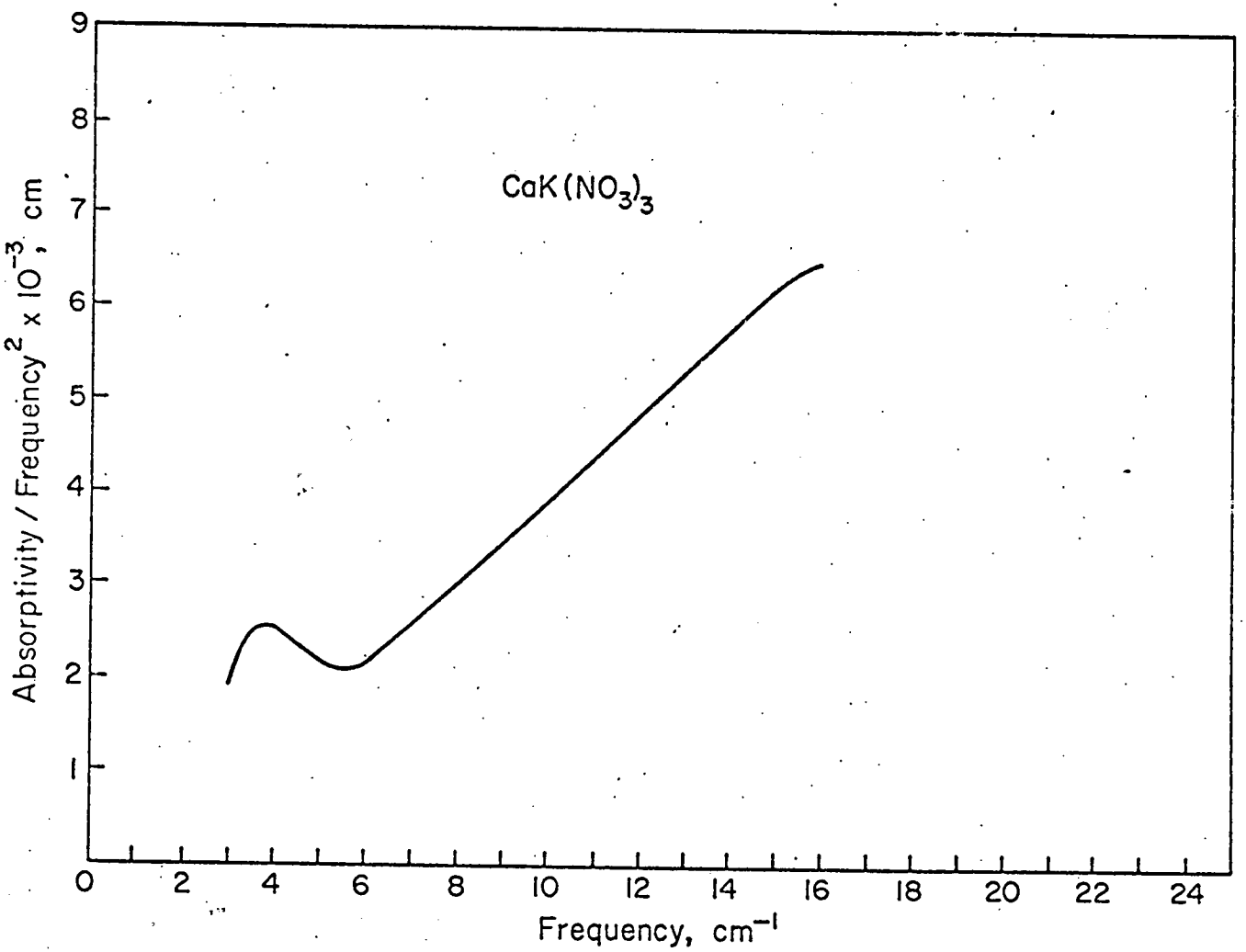

Figure 3.4 The absorption coefficient of vitreous $CaK(NO_3)_3$ plotted as $\alpha(\omega)/\omega^2$ vs. ω.

change from 4.2°K to 1.0°K should increase our absorption coefficient by about a factor of

$$\frac{\tanh(\hbar w/2k(1.0))}{\tanh(\hbar w/2k(4.2))} = \frac{\tanh(4.0k/2.0k)}{\tanh(4.0k/8.4k)} \approx 2.1$$

at a frequency of 2.8 cm^{-1}. The ratio of the transmission at the two temperatures should then be equal to:

$$R = \frac{T(1.0°K)}{T(4.2°K)} = \frac{\ell^{-2.1\alpha d}}{\ell^{-\alpha d}} \approx 0.92 \text{ (at frequencies near 2.8 } cm^{-1})$$

$$R = \frac{T(1.0°K)}{T(4.2°K)} = 1 \quad \text{(at other frequencies)}$$

where α is our measured absorption at 4.2°K. In actual practice changing from 4.2°K to 1.0°K will increase the signal by almost a factor of 2 because the sensitivity of the detector is greater at lower temperatures; but this increase is frequency independent. Our transmission ratio will then be given by:

$$R = \begin{cases} 0.92 \times C \text{ near } 2.8 \text{ } cm^{-1} \\ C \qquad \text{otherwise} \end{cases}$$

where $1 < C \leq 2$. Figure 3.5 shows the ratio of the transmission at 1.0°K divided by the transmission at 4.2°K. One sees that the ratio is frequency independent to within ±5% over our measured range of frequencies, from 2 cm^{-1} to 16 cm^{-1}; which tends to disprove the tunneling model.

Note that we have not proven whether or not the absorption coefficient changes in going from 4.2°K to 1.0°K,

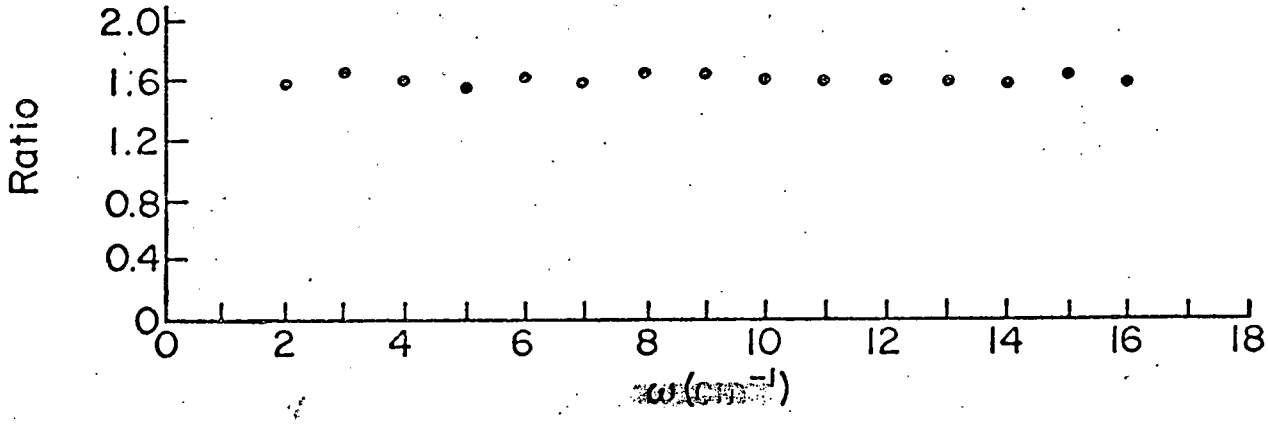

Figure 3.5a

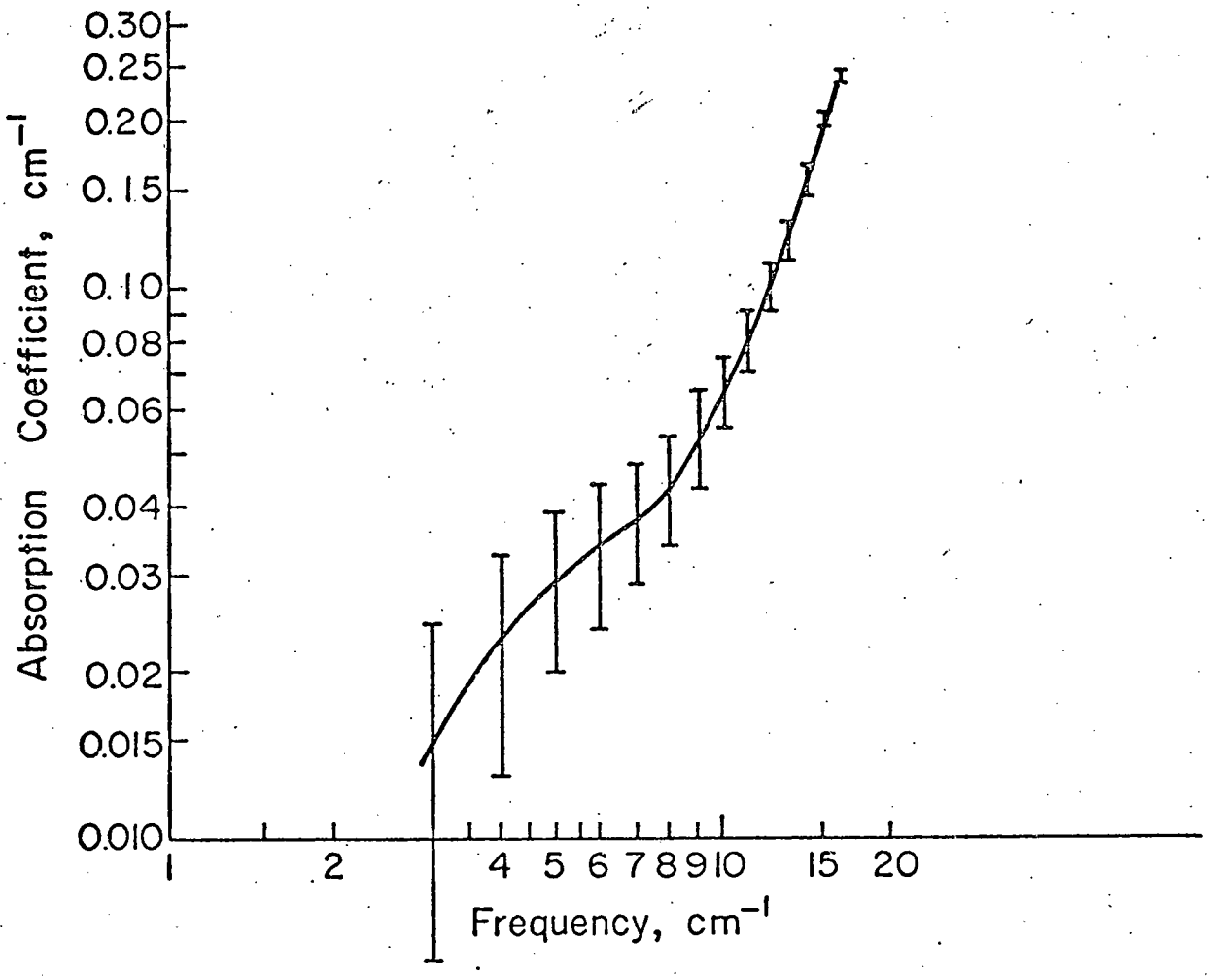

Figure 3.5b

Figure 3.5 a) The ratio of the transmission of a 5.1 cm. long sample of vitreous silica at 1.0°K to the transmission at 4.2°K. The ratio is frequency independent to within ±5%; b) The errors in the absorption due to a ±5% error in the transmission for the 5.1 cm. long sample.

but we have shown that if there is a change the change is constant from 2 cm^{-1} to 16 cm^{-1}, at least to the accuracy of our measurements. Figure 3.5b shows the errors in the absorption due to a ±5% error in the transmission. Although the absolute error in the absorption is constant the percentage error decreases as the value of the absorption coefficient increases (i.e. $\Delta\alpha/\alpha$ is bigger at 3 cm^{-1} then at 16 cm^{-1}).

D. Summary

Our measurements of the absorption coefficient of the three glasses show absorption curves which are qualitatively very similar and do not differ by more than one order of magnitude from each other. In the far infrared region each of our glasses showed two maximas in $\alpha(\omega)/\omega^2$ vs. ω with the respective maxima within ±5 cm^{-1} of each other. Measurements on two different types of vitreous silica showed no noticeable difference. Temperature runs on vitreous silica showed that from 2 cm^{-1} to 16 cm^{-1} the change in the transmission is fairly frequency independent.

CHAPTER IV

CONCLUSIONS

A. Comparison with Others

Figure 4.1 shows a comparison of our data on SiO_2 with the results of other researchers. No comparison can be made for the $CaK(NO_3)_3$ since we have been the first to measure its absorption. Above 10 cm^{-1} there is a good agreement among our various measurements. The SiO_2 samples used by Stolen[6] are G.E. type 101 and 106, those by Whalley[7] are G.E. type 101 and ours are G.E. type 125. It is believed that the difference in our measurements are mainly due to the methods used to derive the absorption coefficient rather than the different impurities[35] in the samples. Below 18 cm^{-1} there appears to be a temperature dependent absorption while at higher frequencies the absorption as measured by Whalley and Stolen shows no temperature dependence. Below 10 cm^{-1} no comparisons are yet possible.

Since there appears to be a temperature dependence of the absorption we have drawn an absorption vs. temperature graph (Figure 4.2) for vitreous silica at several frequencies. The graph is drawn for frequencies of 10 cm^{-1}, 15 cm^{-1} and 20 cm^{-1}, where the points at 4.2°K are from our own data, and at 87°K and 300°K are from Stolen.[6]

Figure 4.1 The absorption coefficient of vitreous silica from our measurements and after R. Stolen[6] and E. Whalley[7].

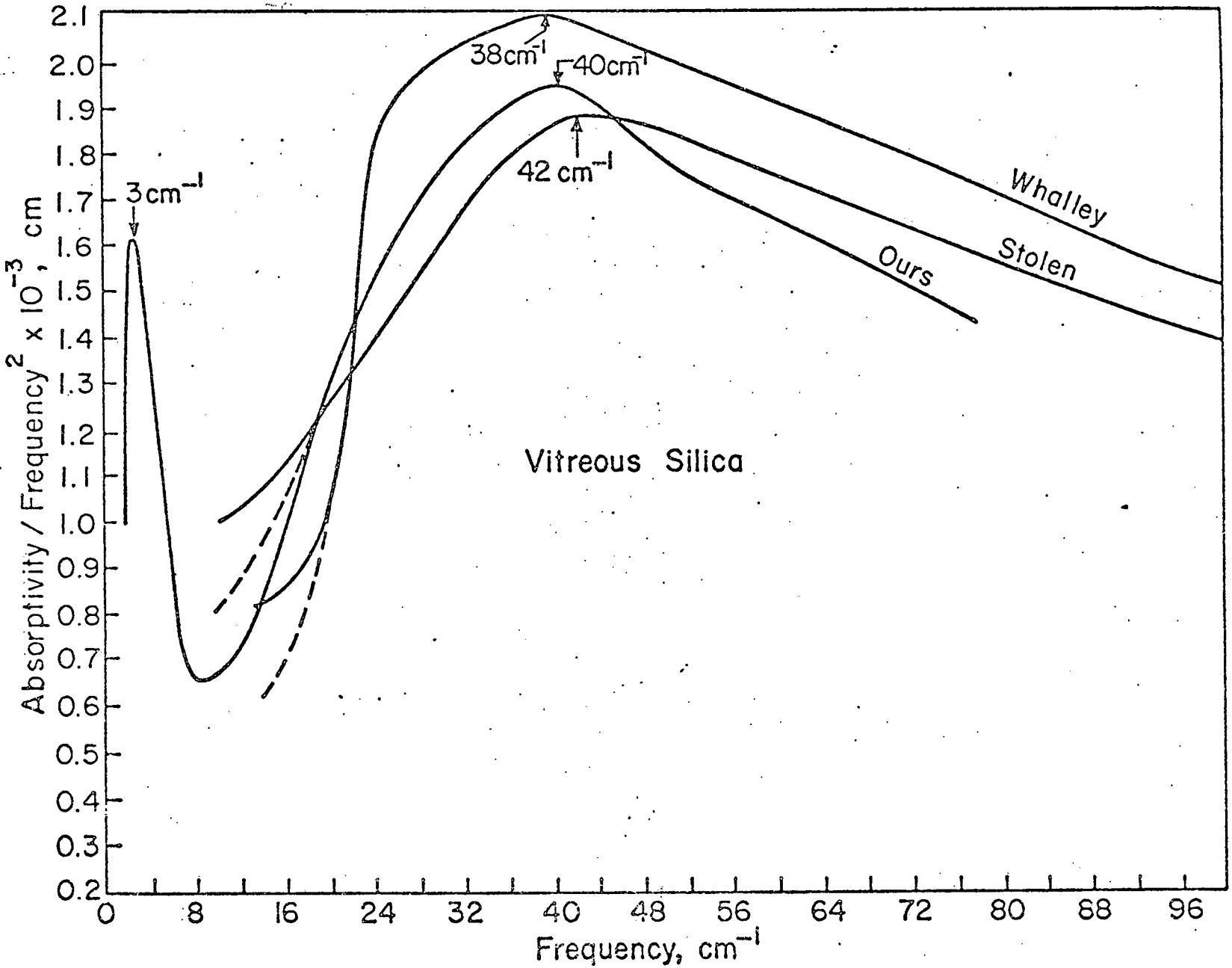
Absorptivity / Frequency^2 x 10^{-3}, cm
Frequency, cm^{-1}
3 cm^{-1}
38 cm^{-1}
40 cm^{-1}
42 cm^{-1}
Whalley
Stolen
Ours
Vitreous Silica
2.1
2.0
1.9
1.8
1.7
1.6
1.5
1.4
1.3
1.2
1.1
1.0
0.9
0.8
0.7
0.6
0.5
0.4
0.3
0.2
0
8
16
24
32
40
48
56
64
72
80
88
96

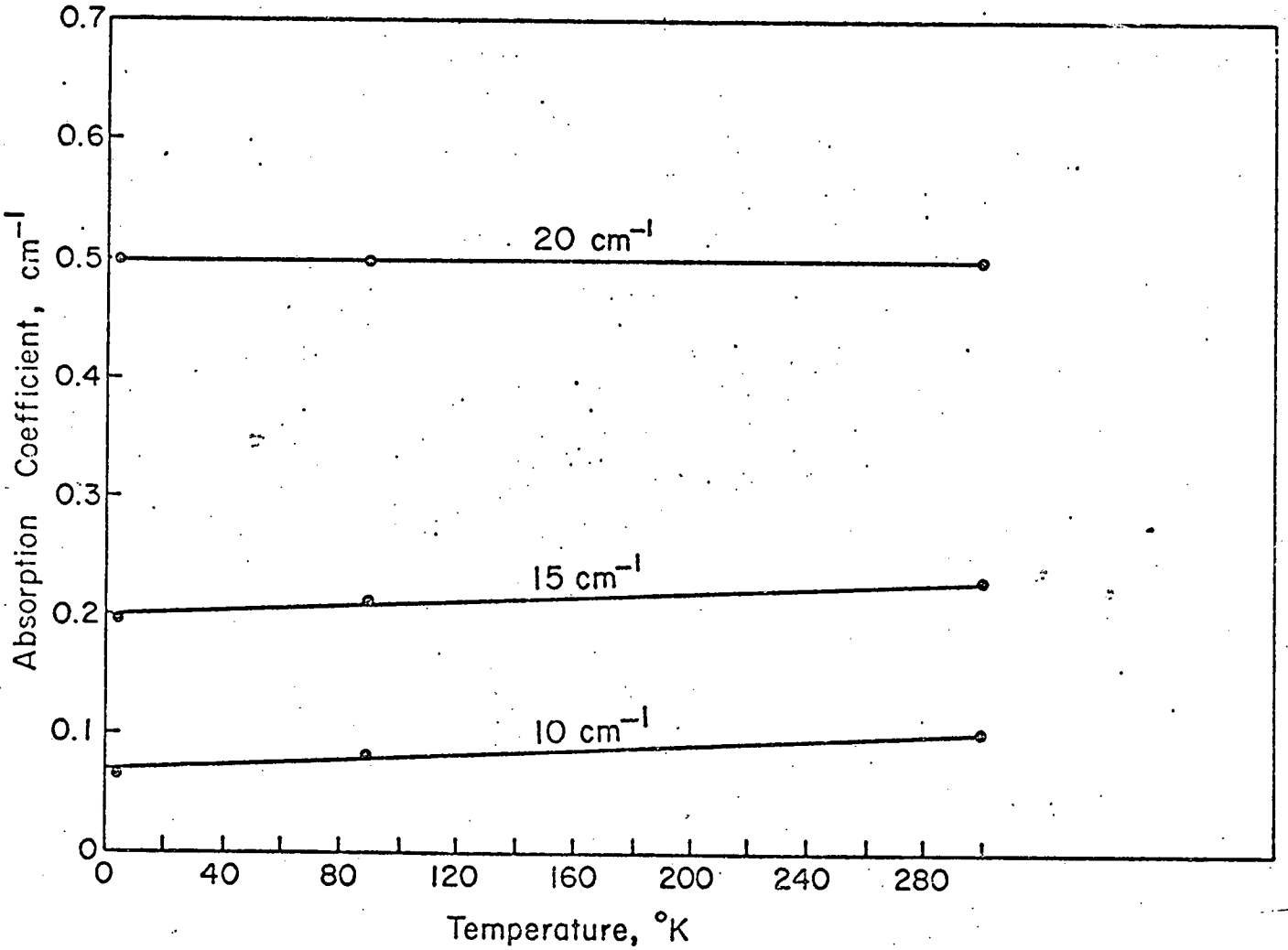

Figure 4.2 The absorption coefficient vs. temperature for vitreous silica at different frequencies; 5 cm^{-1}, 15 cm^{-1} and 20 cm^{-1}. The points at 87°K and 300°K are after R. Stolen.[6]

Looking at Figure 4.2 we see that at a given frequency the absorption increases linearly with the temperature. The slope of the line decreases with increasing frequency so that at 20 cm^{-1} the slope is zero (i.e. the absorption does not depend on the temperature). These results are not very conclusive and precise measurements of the temperature dependence of glasses should be investigated, especially at very low frequencies.

B. Characteristic Spectrum?

One of the questions this thesis has hoped to answer is whether or not a characteristic far infrared absorption spectrum can be associated to glasses. If there is a characteristic spectrum then any theoretical model which attempts to explain the absorption of glasses must be based on properties common to all non-crystalline solids and not on any special features. Measurements of the heat conduction and the specific heat[1,2] have shown that the mechanism determining these properties must be the same for all non-crystalline solids. We will attempt to show that the same is true for the far infrared absorption.

Figure 4.3 shows the absorption vs. frequency data for several non-crystalline solids. The samples are as diverse as SiO_2, GeO_2, $CaK(NO_3)_3$, and B_2O_3.[9] These diverse samples show absorption spectra which are very similar and which do not differ by more than one order

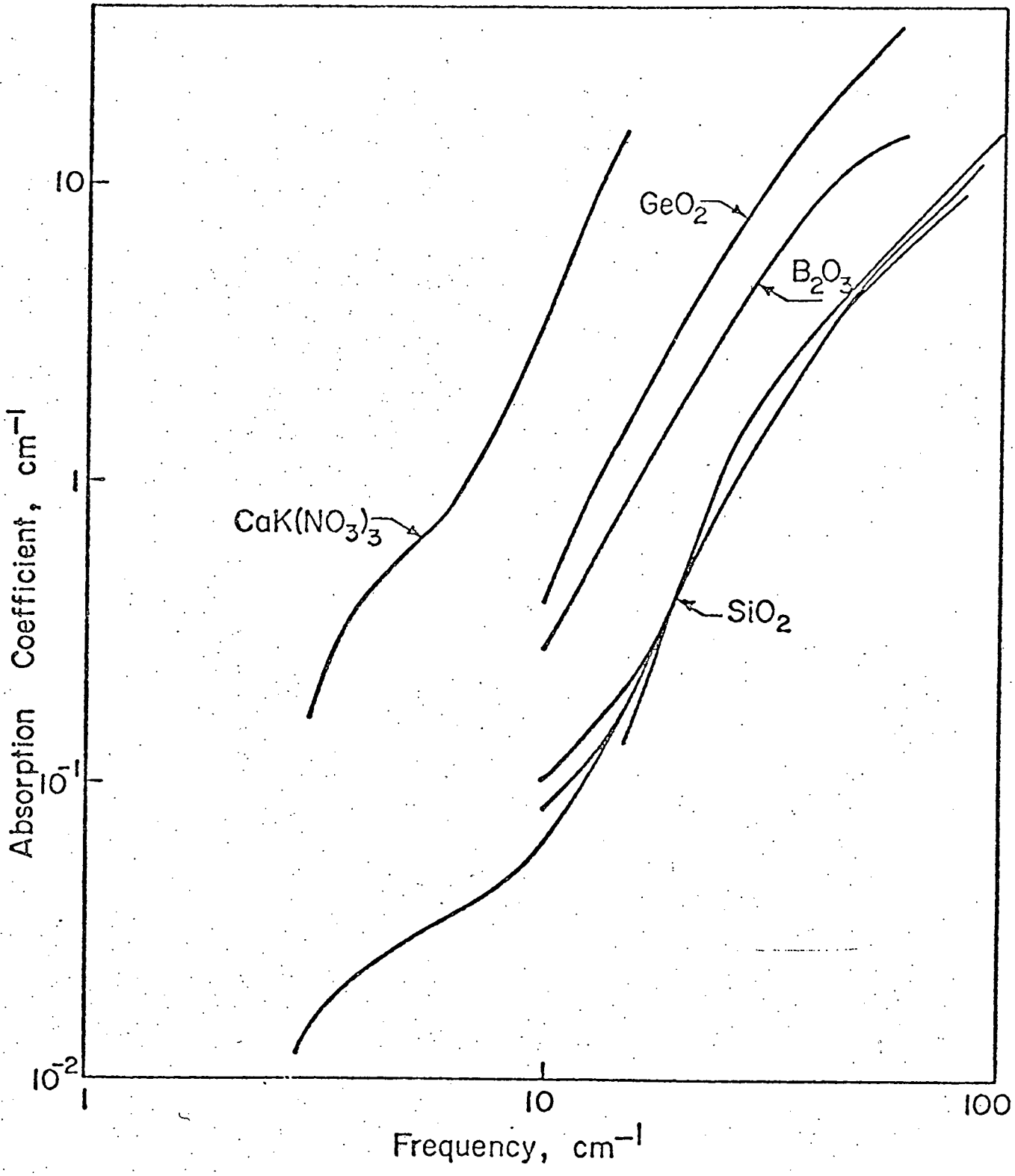

Figure 4.3 The absorption coefficient vs. frequency for several glasses. The data on B_2O_3 are after R. Stolen;[6] those on SiO_2 that begin at 10 cm^{-1} and 15 cm^{-1} are after R. Stolen[6] and E. Whalley[7] respectively.

of magnitude from that of silica glass. This sampling is not as large as that done for the heat conduction measurements where they[1,2] also included AsS_3, Se, Ge No. 7031 varnish, PMMA, PS.

C. Evaluation of Theoretical Models

1. Defects

Stolens[8] proposal that the absorption in glasses is due to defects in the continuous glass appears to be incorrect. His prediction that the absorption should go as the frequency squared (equation 1.1) does not agree with the experimental results (figures 3.2, 3.3, and 3.4). His basic premise that the absorption is due to defects is implausible since a wide variety of samples with different chemical structure, defects, and composition show absorption spectra which are very similar (Figure 4.3).

2. Tunneling States

We have already shown that the temperature dependence of the absorption predicted by a tunneling state model does not agree with our experimental results (Chapter III, section C). Comparing our measurements done at 4.2°K to those done at higher temperatures there appears to be a small increase in absorption with an increase in temperature at frequencies below 18 cm^{-1}. But this change is opposite to that expected by a tunneling state model which predicts a large increase in absorption with a decrease in temperature.

3. Whalley Model

Whalley[7] predicts that for all glasses the absorptivity divided by the frequency squared should be closely related to the density of vibrational states (equation 1.3). To see if Whalley's model is correct we will compare the density of states derived from the absorptivity to that derived by other means, specifically heat capacity and inelastic neutron scattering measurements. Sufficient work has been done on the heat capacity and inelastic neutron scattering of SiO_2, so we will consider the silica glass. Figure 4.4 shows the density of states derived in two ways: The heat capacity divided by the temperature cubed[1] and the absorption divided by the frequency squared (from Figure 3.2) for vitreous silica. Inelastic neutron scattering measurements[36] show a broad peak in the density of states, $P(Q,w)$, at 40 cm^{-1}. The heat capacity measurements show a peak in the density of states at around 36 cm^{-1}. Our measurements in $\alpha(\omega)/\omega^2$ show peaks at 40 cm^{-1} and 3 cm^{-1}. The density of states from the three ways are consistent for the peak around 40 cm^{-1}, but only the absorptivity measurements show another peak at 3 cm^{-1}. It appears that Whalley's basic assumptions are justified around 40 cm^{-1} since he predicts a density of states consistent with other measurements, but the assumptions are not justified at very low frequencies. Whalley's model also fails to predict the observed temperature dependence of the absorption below 18 cm^{-1}.

Figure 4.4 The density of states vs. frequency for vitreous silica. The heat capacity data are after R. Zeller.[1]

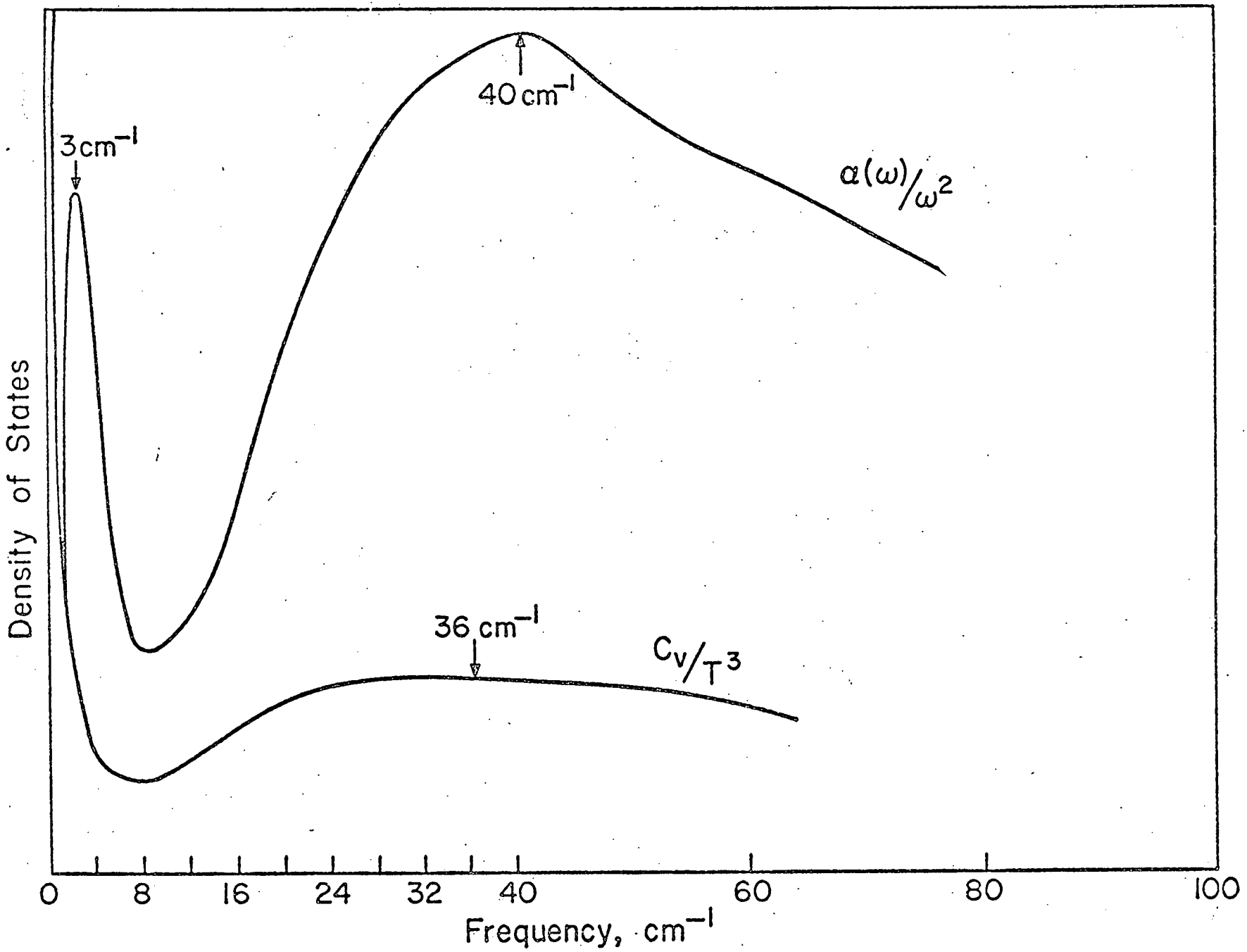
3cm⁻¹
40cm⁻¹
α(ω)/ω²
36 cm⁻¹
Cv/T³
Density of States
0
8
16
24
32
40
60
80
100
Frequency, cm⁻¹

APPENDIX

A. Elimination of Multiple Reflections by Nonparallel Faces

As mentioned in Chapter II, to arrive at an accurate value of the absorption coefficient one must either take into account or eliminate the multiple reflections within the sample. To consider the multiple reflections one uses equation 2.1 which involves knowing the value of the index of refraction at the frequencies where the absorption coefficient is being measured. Since our method for determining the absorption coefficient (equation 2.2) does not depend on knowing the value of the index of refraction, it is more advantageous to eliminate the multiple reflections. This is done by making the faces of the samples non-parallel as shown in Figure A-1.

The way this eliminates the multiple reflections involves using Snell's law and knowing the maximum angle of the radiation which will pass through our light cones to the detector is $18^{\circ}.37$ Our faces were rounded off to at least 2 mm, so the value of θ in Figure A-1 is:

$$\theta \approx \tan \theta = 0.2 \approx 12^{\circ} \quad .$$

Then using Snell's law on the slanted face we have:

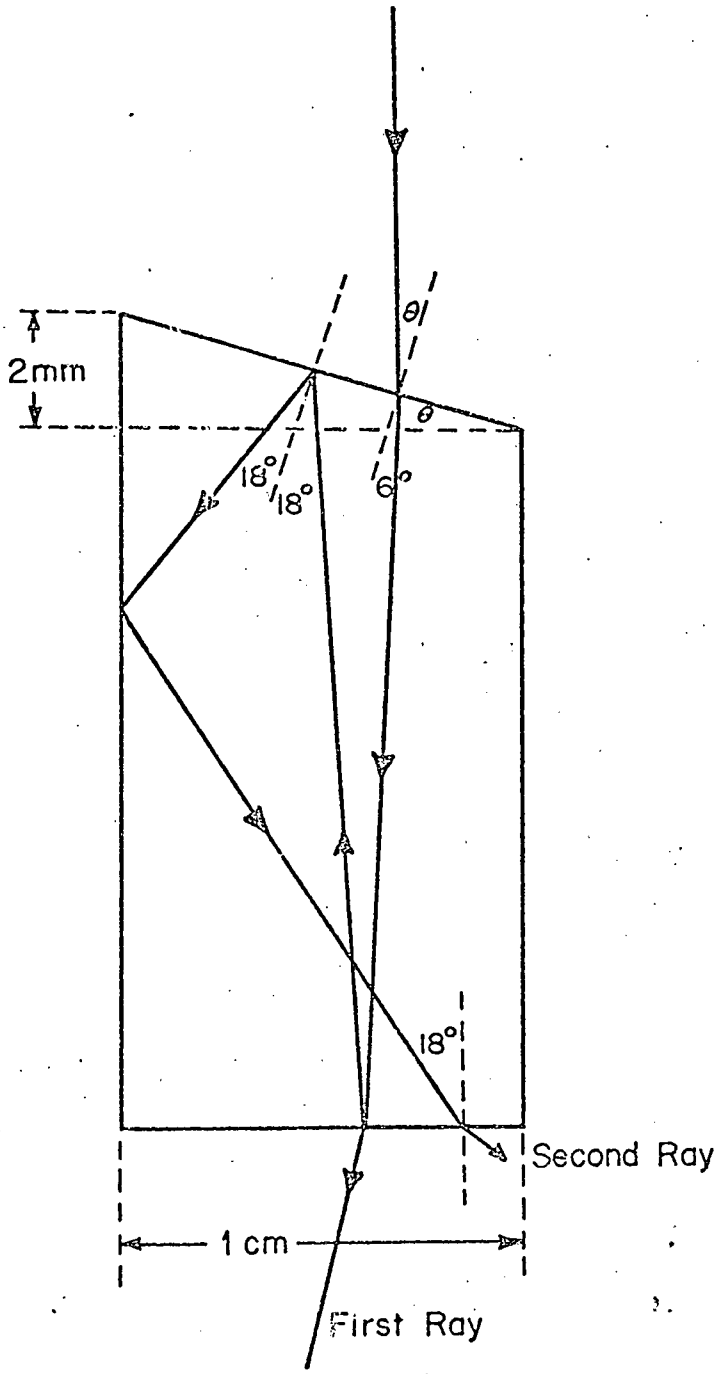

Figure A-1 Transmission through a glass sample with non-parallel faces.

$$n_i \sin \theta = n_2 \sin \theta_2$$

$$1 \cdot (0.2) = 2 \cdot \sin \theta_2$$

$$\theta_2 \approx \sin \theta_2 = 0.1 \approx 6^\circ$$

where we have taken the index of refraction for vitreous silica to be equal to 2. After reflecting off the flat face it will again reflect off the slanted face and thus the reflected angle will be equal to $12^\circ + 6^\circ = 18^\circ$. This angle is further increased when it is refracted from the flat face and the radiation of this second ray will not be able to go to the detector. We have therefore eliminated the multiple reflections.

B. Unsuccessful Experiments

As mentioned in Chapter II when we used 3/8" diameter samples we were getting as much transmission through the long samples as through the short samples at frequencies below 15 cm^{-1}. It was believed that this was due to the absorption of the 3/8" brass sample holders. To eliminate the absorption of the light pipes we platted the light pipes with lead which is a superconductor at $4.2^\circ K$. When we did a run with our samples in these lead-coated sample holders we still had as much transmission through the long samples as through the short samples.

This experiment was not an actual failure because measurements of the absorption of 3/8" light pipes show that the absorption of the light pipes would not produce

such a large effect. That we saw the same effect with the lead platted sample holders confirm the hypothesis that the effect was not caused by the absorption of the light pipes. This effect still remains a puzzle.

REFERENCES

1. R. C. Zeller, M. S. Thesis, Cornell University (1971), Materials Science Center Report No. 1453 and references therein.

2. R. B. Stephens, M. S. Thesis, Cornell University (1973), Materials Science Center Report No. 1969.

3. G. E. Grantham, Ph.D. Thesis, Cornell University (1920).

4. S. S. Ballard, J. S. Browder, J. F. Ebersole, American Institute of Physics Handbook, 3rd ed. (McGraw-Hill, 1972), Chapter 6c.

5. W. Bagdate and R. Stolen, J. Phys. Chem. Solids 29, 2001 (1968).

6. R. Stolen, Phys. and Chem. of Glasses vol. II, no. 3, June 1970.

7. P. T. T. Wong and E. Whalley, Discussions Faraday Soc. 50, 94 (1970).

8. E. M. Amrhein and F. H. Muller, J. of the Amer. Chem. Soc. 90, 3116 (1968).

9. J. Volger and J. M. Stevels, Philips Res. Rep. 11, 452 (1956).

10. L. L. Link and D. B. Herrmann, American Institute of Physics Handbook, 3rd ed. (McGraw-Hill, 1972), Chapter 5d and references contained therein.

11. G. H. Wannier, Elements of Solid State Theory (Cambridge University Press, 1960).

12. H. Bilz and L. Genzel, Z. Physik 169, 53 (1962).

13. J. R. Jasperse, A. Kahan, J. N. Plendl, and S. S. Mitra, Phys. Rev. 146, 526 (1966) and references contained therein.

14. C. D. Lytle, M. S. Thesis, Cornell University (1965), Materials Science Center Report No. 390.

15. A. J. Sievers, Far Infrared Spectroscopy by K. D. Moller and W. G. Rothschild (Wiley-Interscience, 1971), Appendix I and references contained therein.

16. R. A. Westwig, M. S. Thesis, Cornell University (1967), Materials Science Center Report No. 629.

17. E. Schlomann, Phys. Rev. 135, A413 (1964).

18. V. S. Vinogradov, Soviet Phys. Solid St. 2, 2338 (1960).

19. P. W. Anderson, B. I. Halperin and C. M. Varma, Phil. Mag. 25, 1 (1972).

20. W. A. Phillips, Proc. Roy. Soc. Lond., A319, 565 (1970).

21. R. D. Kirby, Ph.D. Thesis, Cornell University (1967), Materials Science Center Report No. 1122.

22. C. D. Lytle, M. S. Thesis, Cornell University (1965), Materials Science Center Report No. 390.

23. I. G. Nolt, R. D. Kirby, C. D. Lytle, and A. J. Sievers, Appl. Opt. 8, 309 (1969).

24. I. G. Nolt, Ph.D. Thesis, Cornell University (1972), Materials Science Center Report No. 765.

25. Digital Equipment Corporation, Maynard, Massachusetts.

26. D. B. Tanner, Ph.D. Thesis, Cornell University (1972), Materials Science Center Report No. 1872.

27. J. J. Taub and H. J. Hindin, Rev. Scient. Instrum. 34, 1056 (1963).

28. P. L. Richards, J. Opt. Soc. Am. 54, 1474 (1964).

29. R. C. Ohlman, P. L. Richards and M. Tinkham, J. Opt. Soc. Am. 48, 531 (1958).

30. Valpey Corporation, Holliston, Massachusetts.

31. Recipe after C. A. Angell, J. Wong, and W. F. Edgell, J. Chem. Phys. 51, 4519 (1969).

32. P. Flusbacker, A. J. Leadbetter, J. A. Morrison and B. P. Sloicheff, J. Phys. Chem. Solids 12, 53 (1959).

33. G. K. White and J. A. Brich, Phys. Chem. Glasses 6, 85 (1965).

34. E. W. Hornung, R. A. Fisher, G. E. Brodale, and W. F. Giaugue, J. Chem. Phys. 50, 4878 (1969).

35. General Electric Specifications and Technical Data.

36. A. J. Leadbetter, J. Chem. Phys. 51, 779 (1969).

37. R. K. Elsley, private communication.